

# A Re-Evaluation of Plasma Shielding

by

Charles Taylor Hansen

A.B. (University of Chicago) 1991

M.A. (University of California at Berkeley) 1993

A dissertation submitted in partial satisfaction of the  
requirements for the degree of  
Doctor of Philosophy

in

Physics

in the

GRADUATE DIVISION

of the

UNIVERSITY of CALIFORNIA at BERKELEY

Committee in charge:

Professor Joel Fajans, Chair

Professor Allan Kaufman

Professor Charles Birdsall

1996

The dissertation of Charles Taylor Hansen is approved:

---

Chair

Date

---

Date

---

Date

University of California at Berkeley

1996

# A Re-Evaluation of Plasma Shielding

Copyright 1996

by

Charles Taylor Hansen

## Abstract

A Re-Evaluation of Plasma Shielding

by

Charles Taylor Hansen

Doctor of Philosophy in Physics

University of California at Berkeley

Professor Joel Fajans, Chair

Plasmas are observed to shield applied perturbations even in the absence of thermal equilibrium. This research examines the dynamics of the velocity distribution function of the plasma which leads to this result. Equilibrium and non equilibrium experiments on a non-neutral plasma are described and the results are compared with the theory of dynamic shielding, developed herein. These experiments were conducted with a Penning-Malmberg trap which is described. Several different types of perturbation are considered. We find that the nonlinear response of the plasma depends strongly on the means by which the perturbation is created. Consequently, some types of perturbations can create unusual and counterintuitive responses in the plasma.

---

Professor Joel Fajans  
Dissertation Committee Chair

To my wife Kelly.

# Contents

List of Figures	vi
<b>1 Introduction</b>	<b>1</b>
1.1 Important Concepts . . . . .	1
1.2 Previous Work . . . . .	4
1.3 Program of research . . . . .	6
<b>2 Theory of Collisionless Shielding</b>	<b>7</b>
2.1 Distribution Functions . . . . .	8
2.2 Constants of the Motion . . . . .	9
2.3 Trapped Charge . . . . .	10
2.4 Two and Three Dimensional Adiabatic Theory . . . . .	13
2.5 One Dimensional Plasmas of Finite Length . . . . .	17
2.6 One Dimensional Plasmas of Finite Radius . . . . .	20
2.7 Instantaneous Trapping . . . . .	26
2.8 Conclusions . . . . .	28
<b>3 The Experiment</b>	<b>29</b>
3.1 Penning-Malmberg Traps . . . . .	29
3.2 The U.C. Berkeley Pure Electron Plasma Trap . . . . .	30
3.3 The Plasma . . . . .	32
3.4 Variation of Parameters . . . . .	32
3.4.1 Density . . . . .	35
3.4.2 The Plasma Space Charge Parameter, $C$ . . . . .	36
3.4.3 Temperature . . . . .	36
3.4.4 Collision Time and Bounce Time . . . . .	36
3.5 Perturbation of the Plasma . . . . .	37
3.6 Diagnostics . . . . .	40
3.7 Measurement of Parameters . . . . .	43
3.7.1 Density . . . . .	43
3.7.2 The Plasma Space Charge Parameter, $C$ . . . . .	44
3.7.3 Temperature . . . . .	44
3.8 Measurement of the Response to a Perturbation . . . . .	46

3.9	Accessible Experiments . . . . .	46
<b>4</b>	<b>Results</b>	<b>48</b>
4.1	Collisional and Collisionless Shielding . . . . .	48
4.2	The Importance of Trapped Charge – Anti-Shielding . . . . .	52
4.3	The Approach to Equilibrium . . . . .	55
4.4	Distribution Functions . . . . .	55
4.5	Conclusions . . . . .	58
<b>5</b>	<b>Conclusions</b>	<b>60</b>
5.1	Applications . . . . .	61
5.2	Future Research Directions . . . . .	62
<b>A</b>	<b>Ongoing Modifications</b>	<b>64</b>
A.1	Fast Perturbations . . . . .	64
A.2	Segmented Filament . . . . .	68
A.3	Vision System . . . . .	70
A.4	Current Progress . . . . .	75
<b>B</b>	<b>Glossary</b>	<b>77</b>
	<b>Bibliography</b>	<b>80</b>

# List of Figures

1.1	Phase space orbits of particles in a potential well . . . . .	3
2.1	A slowly deepening test well, showing how a particle can be trapped . . . . .	12
2.2	The definition of $b$ and $r_{min}$ . . . . .	14
2.3	The deformation of a phase space orbit with increasing perturbation strength	18
2.4	Self-consistent distribution functions . . . . .	21
2.5	“Shielding efficacy”, $1 - \Phi/\Phi_w$ vs. Temperature. . . . .	24
2.6	“Shielding efficacy”, $1 - \Phi/\Phi_w$ vs. applied well voltage. . . . .	25
3.1	Simplified experimental schematic. . . . .	30
3.2	The vacuum potential along the axis of a Penning-Malmberg trap. . . . .	31
3.3	The spiral filament and potentials . . . . .	33
3.4	The injection and trapping sequence . . . . .	34
3.5	The network used to couple the heating signal to the inject gate. . . . .	37
3.6	The final temperature of the plasma as a function of heating signal amplitude	38
3.7	Calculated vacuum potentials for a single cylinder in a Penning-Malmberg trap for two different cylinder aspect ratios . . . . .	39
3.8	An example of the plasma radial profile . . . . .	41
3.9	The wheel and pinhole diagnostic. . . . .	42
3.10	Measurement of the axial distribution of charge by using image charge. . . . .	43
3.11	The variation of the space charge parameter $C$ with temperature . . . . .	45
4.1	Total charge vs. temperature . . . . .	50
4.2	Relative trapped charge vs. temperature . . . . .	51
4.3	Schemes for examining the effect of trapping . . . . .	53
4.4	Relative charge vs. well voltage . . . . .	54
4.5	The plasma approach to equilibrium due to collisions. . . . .	56
4.6	Total charge vs. well voltage at two different times . . . . .	57
4.7	Experimental integrated distribution functions . . . . .	59
5.1	The nested well scheme. . . . .	62
A.1	A diagram of the original construction of the experiment showing some of the difficulties with high speed signals. . . . .	65

A.2	A schematic of the transmission line and gate . . . . .	65
A.3	The response of an open terminated transmission line . . . . .	66
A.4	The response of a transmission line which is terminated with a pure capacitance. . . . .	68
A.5	Comparison between measured and predicted waveforms . . . . .	69
A.6	The layout of the segmented filament . . . . .	70
A.7	Drawing showing the installation of the segmented filament . . . . .	71
A.8	A diagram of the phosphor screen diagnostic . . . . .	71
A.9	The electrode configuration used for electron acceleration . . . . .	72
A.10	The phosphor optics . . . . .	75

## Acknowledgments

There are many people without whom this research might not have occurred. Foremost among them are my fellow graduate students: Anita Reimann, who set up and ran computer simulations to understand various shielding phenomena, who assisted in constructing and running this experiment, and who continues to do so, Ramesh Gopalan, who provided experimental assistance when labor intensive tasks arose, and who provided valuable discussions on ideas both theoretical, experimental, and utterly unrelated to physics, and Dan Durkin. My advisor, Prof. Joel Fajans, deserves credit as well, for although his requests and suggestions sometimes seemed unnecessary when presented, his dedication to experimental excellence made the final product far superior to what it might otherwise have been. I would also like to thank my collaborators in the field of Non-Neutral Plasma Physics for providing valuable sounding boards for our often unconventional and unusual ideas, in particular, Dr. Tom Cowan, Dr. Brett Beck, Jay Hartlee, Prof. Jonathan Wurtele, Prof. Tom O'Neil, Dr. Xiao-Pei Huang, Dr. Steve Crooks, Dr. Kevin Fine, and Prof. Fred Driscoll. I would also like to thank several members of the Plasma Theory and Simulation Group in the EECS department here at Berkeley for providing valuable computer code and even more valuable expertise in running it: Prof. Ned Birdsall, David Cooperberg, and Keith Cartwright.

# Chapter 1

## Introduction

Most elementary discussions of the theory of plasma shielding treat the response of a plasma to a perturbation as a process which occurs in thermal equilibrium without explicit reference to the velocity distribution function. This model is just one of many that might arise experimentally. There are in fact many experimentally observed plasmas where the assumption of thermal equilibrium does not hold. In order to understand the shielding behavior of these plasmas, we must understand the behavior of the particle velocity distribution function under the influence of a perturbation. The following is a theoretical and experimental investigation of several ideas which will allow us to understand plasma shielding in a wide variety of plasmas. The focus of this work is on plasmas which are effectively collisionless, and which, consequently, have a non-Maxwellian particle velocity distribution function when perturbed.

### 1.1 Important Concepts

Charge shielding is one of the most fundamental of plasma physics phenomena, and is generally among the first topics covered in an introductory course [1]. Although not always made explicit, analyses of this phenomenon almost always rely on the assumption that the plasma is in thermal equilibrium and that the electron velocity distribution function is always Maxwellian. This assumption implies that the electron density,  $n_e(x, t)$ , follows the Boltzmann relation:

$$n_e(x, t) = n_{e0} \exp\left(\frac{e\phi(x, t)}{kT}\right). \quad (1.1)$$

When the Boltzmann relation is combined with the assumption of a uniform immobile ion background with  $n_i = n_{e0} \equiv n_o$ , the following self consistent equation for  $\phi$  is obtained:

$$\nabla^2 \phi = \epsilon n_o \left[ \exp \left( \frac{e\phi}{kT} \right) - 1 \right]. \quad (1.2)$$

In introductory treatments this equation is solved approximately by linearizing and applying boundary conditions. A solution to the exact equation can also be obtained by numerical methods.

The key feature of this treatment is that it contains a relation between  $n$  and  $\phi$ , namely the Boltzmann distribution. This type of relation is necessary for any theory of shielding, but this particular relation depends on the fact that the plasma has a Maxwellian distribution function. Since a Maxwellian distribution function arises from thermal equilibrium, and thermal equilibrium is established through collisions, this result may not apply in collisionless plasmas. Let us examine relations between  $n$  and  $\phi$  which do not arise from collisional mechanisms.

Consider the example of an infinite, collisionless plasma in which the electrons are constrained to move in one dimension (by a strong uniform magnetic field, for example.) Assume that this plasma flows through a region where there is a static potential well. Because the energy of the particles is conserved if the depth of the potential well does not change in time, their velocity will increase when they enter the potential well region. The accelerated particles spend less time in the potential well region than they would in an unperturbed region. Hence, the particle density is lower inside the perturbation than outside. This phenomenon can be illustrated by imagining a collection of marbles, all with the same velocity, and with equal spacing between each marble. If this collection of marbles should encounter a downward slope, then the spacing between the marbles will increase as the velocity increases. Thus the density of marbles will decrease as one proceeds downhill. This result is the opposite of the result obtained earlier for the case of thermal equilibrium, where the particle density increases exponentially with the depth of the well. To resolve this apparent contradiction, we examine the phase space diagram shown in Figure 1.1. This phase space diagram clearly shows that there are two classes of orbits, those which close inside the potential well, and those which do not. We will refer to these orbits as trapped and passing (or free) orbits, respectively. The example above implicitly assumed that the trapped orbits are empty. If the trapped orbits could be populated with particles, then the density of particles in the well region might be larger than the density of particles

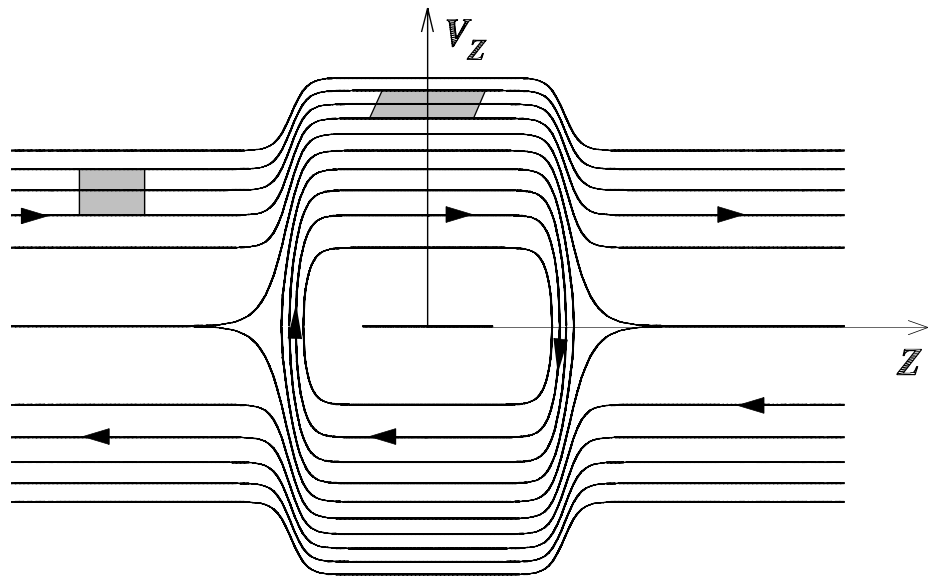


Figure 1.1: Phase space orbits of particles flowing in  $z$  through a potential well region (such as a positive voltage for electrons.) There are two classes of orbits: those which close inside the potential well and those which do not. We will refer to these orbits as trapped and passing orbits, respectively. The density is given by the integral of  $f(v)$  over velocity; hence the density of the shaded bunch of electrons will be lower inside the well than outside. This follows from phase space volume conservation. A group of particles outside the well with average velocity  $v$  and velocity spread  $\delta v$  will have a velocity spread equal to  $(v/v')\delta v$  inside the well (where  $v'$  is the particle velocity inside the well.) Therefore, the spatial extent of this group of particles must increase by a factor of  $v'/v$ . This implies a decrease in density by a factor of  $v/v'$ . This result holds on all passing orbits.

outside the well region, which will have the effect of screening the well. The difficulty lies in discerning the mechanism by which the trapped orbits become populated. In thermal equilibrium, collisions cause particles to move from orbit to orbit in phase space, and can cause particles to move from passing to trapped orbits, but in collisionless plasmas, this mechanism does not occur.

The problem is now clear. In order to resolve the apparent contradiction of a one dimensional perturbation, we must find a collisionless mechanism by which particles can become trapped in a potential well. The process of particle trapping will determine the particle distribution function in phase space,  $f(v)$ , both inside and outside the well. The distribution function can then be used to find the density and thus determine the plasmas response to a perturbation which is analogous to the Maxwell-Boltzmann relation. This extra step of examining the dynamics of the distribution function explicitly is necessary in collisionless plasmas where a thermal distribution can no longer be assumed.

## 1.2 Previous Work

There has been much theoretical work on plasma perturbations in general and plasma shielding in particular which is relevant to the present experiments. This previous work generally falls into three categories. The first category assumes that the plasma is in thermal equilibrium with a Maxwellian velocity distribution function for the entire process. The theory of Debye shielding as taught in introductory textbooks on plasma physics ([1, 2], for example) falls into this category. The second category of calculation is valid for perturbations which occur on time scales that are much shorter than the orbital period of the plasma particles [2, 3, 4, 5, 6]. These calculations are similar to many calculations of wave particle interactions – they rely on linearizing the Vlasov equation, or equivalently, linearizing the equations of motion. Although the requirement of thermal equilibrium is no longer needed, the linearization of the Vlasov equation involves some additional assumptions. First order perturbations of the Vlasov-Poisson system not only require that the perturbation be small, they also require that passing orbits remain passing. The linear perturbation theory is no longer valid when, for example, the particles begin to bounce inside the well of the perturbation. Linearization places a limit not only on the amplitude of the perturbation, but also on the time over which the solution is valid. The linear approximation is therefore valid for a time much less than a trapped particle bounce period. For the sake of clarity,

we will refer to these rapid perturbations as “instantaneous” perturbations.

Although the method of determining the response to a perturbation is very different in the equilibrium and instantaneous calculations, the objects of the two are very similar. A relation between the plasma density and the potential is found, which, along with the Poisson equation, allows the problem to be solved. One very important result of both of these theories is that they possess the same small perturbation potential,  $e\phi \ll kT$  limit.

The equilibrium and instantaneous theories are theories of shielding which are commonly presented in textbooks. Although they provide similar results when in the limit of small perturbation potential, their extensions to the regime where the potential energy of the plasma particles in the perturbation is comparable to or larger than their thermal energy differ radically (as will be shown in Chapter 2.) Implicit in both of these theories is the idea that particles can become trapped in the potential well created by the perturbation – in the first case, through collisions, and in the second case, through the prior presence of particles in the region where the well is to be created and the inability of these particles to leave this region until after the perturbation is applied. The third category of shielding theory requires that we consider the problem of trapping explicitly.

One type of particle trapping in a negative potential well has been extensively studied by Gurevich [7], who assumes that the perturbation is applied on a time scale which is slow compared to the individual particle motion but fast enough for collisions not to have an effect. We refer to this type as “adiabatic.” This trapping phenomenon is common in the experiments to be discussed later; hence we will develop the theory of adiabatic trapping extensively in Chapter 2. Although adiabatic trapping has been previously analyzed, the implications for shielding have not been explored. Our initial state of knowledge is summarized in Table 1.1. One of the aims of this thesis is to extend the

Time Domain:	Collisional	Collisionless	Orbital
Trapping Mechanism:	Equilibrium	Adiabatic	Instantaneous
Implications for Shielding:	Understood	Not Understood	Linear Limit Only

Table 1.1: A summary of the past understanding of shielding for various time domains.

theory of shielding to all three time domains listed in table 1.1.

In addition to the calculations mentioned above, there have been calculations of the effects of the dimension of the perturbation, i.e. whether the plasma being perturbed

has one two or three dimensions, or equivalently, whether a three dimensional plasma is perturbed by a plane charge, a line charge, or a point charge. [8, 9, 10, 11]. A summary of these ideas is found in the work of Meyer-Vernet [12]. Meyer-Vernet's calculation ignores the origin and time scale of the perturbation and considers only the consequences of conservation of particle flux in one, two and three dimensions; the analysis is based on the manner in which the trajectories of the particles in the plasma change in response to the perturbation. The change in trajectories leads to a change in density which changes the potential. One critical idea summarized in Meyer-Vernet's analysis is that the change in trajectories will be different if the dimensionality of the model is different. Consequently, it is necessary to treat the cases of point charge, line charge and plane charge perturbations separately. It is important to note that geometrical analyses such as Meyer-Vernet's do not include the trapped particle trajectories, namely those which do not connect to the unperturbed plasma. Although we find experimentally that there are cases where trapped orbits are unpopulated, it is generally the case that one or more of the trapping mechanisms above will be important. Thus a complete theory of shielding must contain considerations of both geometrical configuration and trapping.

### 1.3 Program of research

The remainder of this thesis will develop these models in detail. We will begin by examining the theory of plasma shielding more fully in Chapter 2. The goal of this analysis will be to predict the results of experiments in which perturbations like the ones discussed above are applied to a pure electron plasma. The device on which these experiments were performed is discussed in Chapter 3; this chapter begins with a general description of Penning-Malmberg traps, and concludes with a detailed description of the U.C. Berkeley pure electron plasma trap. Chapter 4 presents the results of these experiments and compares the results with theory. Finally, Chapter 5 discusses the importance of the results obtained in the other chapters and speculates on some future applications for the theory. In Appendix A we discuss some hardware modifications and upgrades which are now in progress. Appendix B is a glossary of terms which are used in this thesis.

## Chapter 2

# Theory of Collisionless Shielding

This chapter describes the theory of shielding in collisionless plasmas in two limits where analytic results can be obtained. In both these limits, the plasma is not in thermal equilibrium, so the methods of equilibrium statistical mechanics can not be used. The theories presented in this chapter take into account both the time scale of the perturbation and the geometrical properties of the plasma.

Two time scales in the problem are the collision time and the period of the bounce orbits of the particles. As we discussed in Section 1.2, perturbations which occur in a time much slower than the electron-electron collision time can be understood by assuming that the electrons remain in thermal equilibrium with each other throughout the perturbation process. (A similar theory can be used for the ions in a multi-species plasma.) The main focus of this chapter will be on perturbations which occur on time scales much faster than a collision time yet much slower than an orbit time. At the end of the chapter, we will extend some of the aspects of the rapid time scale theory to cover some problems that will arise in our experiment.

Section 1.2 also discussed some of the work that has been done to determine the effect of the dimensionality of the perturbation on the response. In this chapter, we will combine this with the theory of collisionless trapping to present a more complete picture of the theory of shielding in one, two and three dimensions. The theory of one dimensional shielding is of particular interest to us due to the fact that our experiment is essentially one dimensional. (This will be explained further in Chapter 3.) Furthermore, to compare theory with experiment, it will be necessary to extend the theory of one dimensional trapping to finite size plasmas.

## 2.1 Distribution Functions

The processes we wish to describe are non equilibrium processes, therefore the concept of temperature is not valid. We must therefore model the changes in the velocity distribution function  $f(x, v)$  in detail. (Note that for simplicity, we are considering a one dimensional distribution, and  $v$  is the magnitude of the particle velocity.) The plasma density and other relevant quantities can then be calculated from  $f(x, v)$ .  $f(x, v)$  has the important property that it must be a solution to the Vlasov equation. In the cases to be considered below,  $f(x, v)$  is assumed to be either stationary, or quasi stationary in time, meaning that changes in  $f(x, v)$  are slow with respect to both  $1/\omega_p$ , and the period of the orbital motion of the particles, which implies that the time derivative in the Vlasov equation can be neglected.  $f(x, v)$  therefore satisfies the equation

$$v \cdot \frac{\partial f}{\partial x}(x, v) + \frac{e}{m} E_{\parallel}(x) \frac{\partial f}{\partial v}(x, v) = 0. \quad (2.1)$$

Note that we are considering only the magnitude of the velocity parallel to  $\mathbf{B}$ , which we assume to lie in the  $\hat{x}$  direction.

The analysis is simplified if constants of the motion can be found. By constants of the motion, we mean quantities which are conserved (or approximately conserved) over a single orbit. Suppose  $f(x, v)$  can be written as a function only of some set of constants of the motion,  $\alpha_i(x, v)$ , so that

$$f = f(\alpha_1(x, v)) \quad (2.2)$$

(In higher dimensions  $f = f(\alpha_1(x, v), \alpha_2(x, v), \dots)$ .) The Vlasov equation then becomes

$$\sum_i \frac{\partial f}{\partial \alpha_i} \left[ v \frac{\partial \alpha_i}{\partial x} + \frac{e}{m} E_{\parallel}(x) \frac{\partial \alpha_i}{\partial v} \right] = 0 \quad (2.3)$$

Since each  $\alpha_i$  is a constant of the motion, each term in brackets vanishes independently. Therefore, any  $f$  which is a function only of the constants of the motion is a time independent solution of Vlasov's equation. The purpose of finding these constants of the motion is to understand how the orbits of the particles change under the influence of a perturbation. The goal will be to obtain a complete description of the orbit using these constants, and then determine how the orbit will change under the influence of a perturbation by finding the new constants of the motion after the perturbation has been applied.

## 2.2 Constants of the Motion

If we assume that the particle is constrained to move in only one dimension, then only one constant of the motion is required to completely describe the particle orbit. If we assume that the electric potential does not vary in time, then the total energy (kinetic plus potential) of a particle is conserved. The energy, therefore, is one obvious choice for a constant of the motion. It is often more convenient, however, to pick the velocity of the particle at one point in the trap as our constant. This velocity, along with energy conservation, determines the particle velocity everywhere. We can further simplify the problem by choosing this same point to define zero potential energy. (Note that this implies that all the particles are free or passing particles.) Thus our constant of the motion,  $v_o$ , is defined by:

$$v_o(x, v)^2 = v^2 - 2\Phi(x). \quad (2.4)$$

Note that  $v$ ,  $v_o$ , and  $\Phi$  are all normalized quantities, defined as follows:  $v$  ( $kT/m$ )<sup>1/2</sup> has units of velocity and  $\Phi$  ( $kT/e$ ) has units of electrical potential. Note also that we assume that the velocity distribution is symmetric, and consider only the magnitude of  $v_o$ . This is done to simplify expressions which appear later. We have also assumed that the particles have a negative charge.

Since  $v_o$  is a constant of the motion,  $f(v_o)$  determines  $f(v)$  everywhere. Using equations 2.2 and 2.4 gives

$$f(x, v) = f(v_o(x, v)) = f\left(\sqrt{v^2 - 2\Phi(x)}\right). \quad (2.5)$$

To illustrate, suppose that the plasma consists only of particles streaming in from a Maxwellian source at  $\Phi = 0$  far away from any potential variations. This implies that

$$f(x, v) = \frac{n_o}{\sqrt{\pi}} \exp\left(-v_o^2/2\right) = \frac{n_o}{\sqrt{\pi}} \exp\left(-\left(v^2/2 - \Phi(x)\right)\right) \quad (2.6)$$

where  $n_o$  is the electron density where  $\Phi = 0$ . To find the density everywhere, we integrate  $f(v)$  over all possible orbits. If we only allow perturbations in  $\Phi$  which form potential wells ( $\Phi \geq 0$ ) rather than potential hills ( $\Phi < 0$ ), then

$$n(x) = \int_{v_o=0}^{\infty} f(v_o(v, x)) dv = \int_{\sqrt{2\Phi}}^{\infty} \frac{n_o}{\sqrt{\pi}} e^{-(v^2/2 - \Phi)} dv = n_o \exp(\Phi) \left[1 - \operatorname{erf}\left(\sqrt{\Phi}\right)\right]. \quad (2.7)$$

Note that by assuming a Maxwellian distribution where  $\Phi = 0$ , we have assumed that all orbits connect with the region where  $\Phi = 0$ , which means that all the particles are on

orbits with energy greater than zero. Since we have assumed  $\Phi \geq 0$  everywhere, none of the particles are trapped in a potential well. Since  $n(x) \leq n_o$  we see that a population consisting entirely of untrapped electrons will always decrease in density in a potential well.

The analysis above assumes that the potential is known everywhere. In general, the potential can be broken down into two parts, the part which is due to the plasma itself and the part which is due to external influences. Since the potential becomes more positive in a region with fewer electrons, the effect of a decrease in electron density in a region of positive potential will be to cause the total potential to be larger in magnitude than the applied potential. In this case, the potential well will be “anti-shielded.”

## 2.3 Trapped Charge

The conclusion that the well will be anti-shielded is a consequence of the fact that no charge is trapped in it. However, as was noted in section 1.1, the manner in which a well is created can trap charge. In general, the only way to observe anti-shielding is to create the well before the plasma flows into it. If there is plasma in the vicinity of the well at the time when the well is created, there are always collisionless mechanisms which will trap charge. This is a straightforward consequence of the conditions under which conservation of energy holds in an electrostatic system. To illustrate this, suppose that we have a particle of charge  $q$  moving in an electrostatic field. The equation of motion is

$$m \frac{d\mathbf{v}}{dt} = q\mathbf{E}(x, t). \quad (2.8)$$

Multiplying both sides by  $\mathbf{v}$  gives

$$\frac{m}{2} \frac{d\mathbf{v}^2}{dt} = q\mathbf{E}(x, t) \cdot \mathbf{v} = -q\mathbf{v} \cdot \nabla\phi(x, t). \quad (2.9)$$

When the total derivative is written as a convective derivative,

$$\frac{\partial}{\partial t} \left( \frac{1}{2} m\mathbf{v}^2 \right) + \mathbf{v} \cdot \nabla \left( \frac{1}{2} m\mathbf{v}^2 + q\phi(x, t) \right) = 0. \quad (2.10)$$

When  $q(\partial\phi/\partial t)$  is added to both sides of the equation,

$$\frac{\partial}{\partial t} \left( \frac{1}{2} m\mathbf{v}^2 + q\phi(x, t) \right) + \mathbf{v} \cdot \nabla \left( \frac{1}{2} m\mathbf{v}^2 + q\phi(x, t) \right) = q \frac{\partial\phi}{\partial t}(x, t). \quad (2.11)$$

Therefore

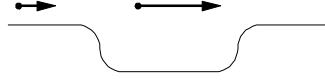
$$\frac{d}{dt} \left( \frac{1}{2} m\mathbf{v}^2 + q\phi(x, t) \right) = q \frac{\partial\phi}{\partial t}(x, t). \quad (2.12)$$

Equation 2.12 implies that whenever a charged particle enters a region where  $\phi(x,t)$  is changing in time, its total energy will no longer be conserved. In particular, if  $\phi(x,t)$  is increasing, the total energy of an electron ( $q < 0$ ) will be decreasing in time. This means that an electron with a sufficiently low initial energy can be trapped by the change in the potential.

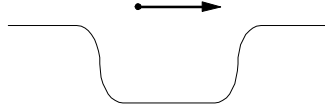
In our experiments, the most common trapping mechanism is the transit time, or adiabatic mechanism first discussed by Gurevich [7], and mentioned briefly in section 1.1. The process is easily visualized for square test wells, but may occur for any shape well. Consider a slowly deepening square test well located in an infinite one dimensional plasma. By slowly deepening we mean that nearly all of the particles traverse the well quickly in comparison to the time it takes for the well to be formed. We will assume that although most particles traverse the well quickly so their total energy is not greatly affected by the slow changes in the well, there will be particles with a velocity infinitesimally close to zero which will be affected by the changes in the well. A low velocity particle will feel an accelerating force as it enters the test well and it will gain kinetic energy. As it traverses the flat bottom of the well, it feels no force even though the well is becoming deeper. Its kinetic energy will therefore not change, but its total energy will. By the time the particle has reached the far edge of the well, it may no longer have enough total energy (kinetic plus potential) to climb out of the well. It will therefore be reflected and trapped. This process is illustrated in Figure 2.1. Once a particle has become trapped in a square well, the only forces it feels are the forces which cause it to be reflected from each edge. Since the net impulse imparted by these forces does not depend on the depth of the well, the kinetic energy of a trapped particle does not change as the well gets deeper. Since we have assumed that the perturbation is increased slowly, only the very slowest particles in the plasma will be trapped. Therefore, for an arbitrarily slow perturbation, the phase space density of the trapped particles is simply the density of particles in phase space with velocity equal to zero.

We have assumed that the plasma is infinite in length. This means that any particle which transits the well region without being trapped will never again encounter the well. Furthermore, all of the particles which do enter the well region have never done so before. Therefore, we assume that the phase space distribution  $f(v)$  of untrapped particles just outside the perturbation is not affected by the perturbation. Consequently, as the well gets deeper, each orbit that becomes trapped will have the same density of particles in

The particle accelerates as it enters the well:



The particle feels no force as it transits even though the well lowers:



By the time the particle has reached the opposite side, the well is too deep to escape:

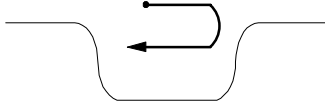


Figure 2.1: A slowly deepening test well, showing how a particle can be trapped

phase space. The resulting distribution function in the well will be

$$f(v) = f_o(0) \text{ for } v \leq \sqrt{2\Phi}, \quad (2.13)$$

where  $\Phi$  is the final depth of the well. After the well has been created,  $\Phi$  no longer varies in time. Energy conservation can be used to find the density of particles on orbits where  $v > \sqrt{2\Phi}$ .

$$f(v) = f_o \left( \sqrt{v^2 - 2\Phi} \right). \quad (2.14)$$

where  $f_o$  is the distribution function outside the well. To find the density as a function of potential, we integrate these distribution functions over velocity.

$$n(\Phi) = \int_0^{\sqrt{2\Phi}} f_o(0) dv + \int_{\sqrt{2\Phi}}^{\infty} f_o \left( \sqrt{v^2 - 2\Phi} \right) dv. \quad (2.15)$$

With the assumption that the distribution function outside the well,  $f_o$ , is Maxwellian, these integrals can be evaluated exactly, so therefore,

$$n(\Phi) = 2n_o \sqrt{\Phi/\pi} + n_o \exp(\Phi) \left[ 1 - \operatorname{erf} \left( \sqrt{\Phi} \right) \right]. \quad (2.16)$$

The potential due to both the externally applied well and the space charge (the self consistent potential) can now be found everywhere by substituting this relation into the Poisson

equation as was done for the equilibrium case in Section 1.1. We obtain a differential equation for  $\Phi$ ,

$$\frac{\partial^2}{\partial x^2}\Phi = \frac{1}{\lambda_D^2} \left( 2\sqrt{\Phi/\pi} + \exp(\Phi) \left[ 1 - \operatorname{erf}(\sqrt{\Phi}) \right] - 1 \right). \quad (2.17)$$

Note that in the limit  $\Phi \ll 1$ , we obtain

$$\frac{\partial^2}{\partial x^2}\Phi = \frac{1}{\lambda_D^2} \left( 2\sqrt{\Phi/\pi} + \left[ 1 - 2\sqrt{\Phi/\pi} + \Phi + \dots \right] \right) \simeq \frac{1}{\lambda_D^2}\Phi, \quad (2.18)$$

therefore, for a small well, this response is nearly identical to the Debye response. Since for large  $\Phi$  the right hand side of Equation 2.17 is significantly smaller than in the Debye case (see Equation 1.2) i. e.

$$\exp(\Phi) \gg 2\sqrt{\Phi/\pi} + \exp(\Phi) \left[ 1 - \operatorname{erf}(\sqrt{\Phi}) \right] - 1, \quad (2.19)$$

for a large well, the response is significantly weaker than the Debye case.

The above analysis has assumed that  $\Phi \geq 0$ , a potential well. The analysis is different if the perturbation forms a potential hill instead of a potential well [12, 13]. In the case of a potential hill, there is no trapped charge, but there is a region in  $x$  space that excludes some of the particles. The distribution will be the same as the free charge distribution in Equation 2.5 (but now of course  $\Phi < 0$ .) The limits of integration change however. In this case, we have

$$n(\Phi) = \int_0^\infty f(\sqrt{v^2 - 2\Phi}) dv. \quad (2.20)$$

For a Maxwellian plasma outside the well, one obtains

$$n(\Phi) = n_o \exp(\Phi), \quad (2.21)$$

which is exactly the same result as would be obtained by assuming thermal equilibrium throughout. In the case of a potential hill, therefore, the result for shielding will be exactly the same as the result of the Debye calculation.

## 2.4 Two and Three Dimensional Adiabatic Theory

The theory of shielding in two and three dimensions differs significantly from the theory of shielding in one dimension. Nevertheless, several concepts from the previous

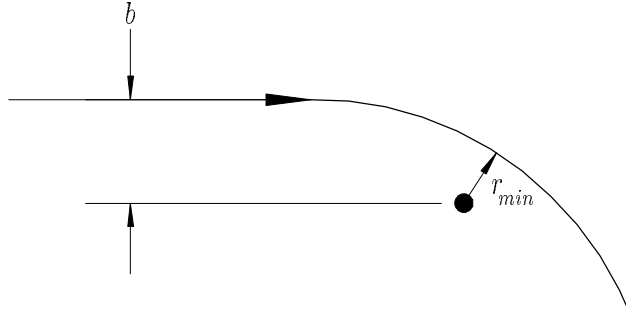


Figure 2.2: The definition of  $b$  and  $r_{min}$ .

sections can be profitably employed. When the plasma electrons are no longer constrained to move in one dimension, their orbits will be deflected towards a positive perturbation and away from a negative perturbation. This bending of orbits increases the local density, which has the opposite effect as the change in the velocity of the particles. This orbit bending effect has been studied extensively [12, 14], but it is not the only mechanism which can cause a change in the charge density in the vicinity of a perturbation. Particle trapping can also play a significant role. The combination of these two mechanisms will be examined in the following section.

We will begin by summarizing the effect of the bending of particle orbits on the density. To simplify the analysis, we will first consider the effect of a stationary test charge (with its self consistent potentials) on a collection of particles which all have the same velocity vector, but which have a uniform density in space far from the test charge (i. e. where  $\Phi = 0$ ). We will then average the effect over all velocity directions and all velocity magnitudes to obtain the response of the plasma.

Suppose the particles all have velocity vector  $\mathbf{v}_o$ , with magnitude  $v_o = \|\mathbf{v}_o\|$ . Energy conservation implies that the magnitude of the velocity of all the particles will be given as a function of the distance from the test charge by:

$$v(r) = \sqrt{v_o^2 + 2\Phi(r)}. \quad (2.22)$$

Since angular momentum is conserved, a particle with impact parameter  $b$  will have a distance of closest approach given by:

$$r_{min} = \frac{bv_o}{v(r_{min})} = \frac{bv_o}{\sqrt{v_o^2 + 2\Phi(r_{min})}}. \quad (2.23)$$

(See Figure 2.2.) This distance of closest approach defines a sphere centered on the test charge in the case of a three dimensional perturbation and a circle centered on the test charge in the case of a two dimensional perturbation. Any particle which has an impact less than  $b$  will cross this sphere or circle. To find the density as a function of distance from the perturbation, we determine the flux of particles with impact parameter less than  $b$  and equate this to the flux of particles crossing  $r_{min}$ . This will provide a relation between the density of particles at infinity and the density of particles at  $r_{min}$ .

We now consider all the particles with velocity magnitude  $v_o$  (effectively averaging over all directions.) We wish to find the number of these particles which are incident on the surface defined by  $r_{min}$  (e. g. the sphere of radius  $r_{min}$  in the case of three dimensions) per unit time in terms of the density at this surface:

$$N(r_{min}, v_o) = \frac{n(r_{min}, v_o)}{2} \langle v_{\perp}(r_{min}) \rangle A_r(r_{min}), \quad (2.24)$$

where  $A_r(r_{min})$  is the area or length defined by the distance of closest approach,  $r_{min}$ , and  $\langle v_{\perp} \rangle$  is the average component of the velocity of the particles perpendicular to the sphere or circle for all particles with initial velocity  $v_o$ . Since the trajectory of each of these particles must have originated at a point with impact parameter less than  $b$ ,  $N(r_{min}, v_o)$  must also be given by:

$$N(r_{min}, v_o) = n_o(v_o)v_o A_b(b) \quad (2.25)$$

where  $A_b(b)$  is the surface area or length defined by the impact parameter  $b$ . We can now solve these equations for  $n(r_{min}, v_o)$  given the appropriate expressions for  $\langle v_{\perp}(r_{min}) \rangle$ ,  $A_r(r_{min})$ , and  $A_b(b)$ , for two and three dimensions.

In two dimensions,

$$\langle v_{\perp}(r_{min}) \rangle = \langle \mathbf{v}(r_{min}) \cdot \hat{n} \rangle = v(r_{min}) \cdot \frac{\int_{-\pi/2}^{\pi/2} \cos(\theta) d\theta}{\int_{-\pi/2}^{\pi/2} d\theta} = \frac{2}{\pi} \cdot v(r_{min}), \quad (2.26)$$

$$A_r(r_{min}) = 2\pi r_{min}, \quad (2.27)$$

and

$$A_b(b) = 2b. \quad (2.28)$$

Substituting these into equations 2.24 and 2.25 gives

$$n_o(v_o)v_o \cdot (2b) = \frac{n(r_{min}, v_o)}{2} \left( \frac{2}{\pi} \cdot v(r_{min}) \right) 2\pi r_{min}. \quad (2.29)$$

Therefore,

$$\frac{n(r, v_o)}{n_o(v_o)} = \frac{bv_o}{rv(r)} = 1 \quad (2.30)$$

by angular momentum conservation [12]. Therefore, for every initial velocity, the density of the untrapped particles does not change. The trapped charge will be a very different story. By analogy to the method in section 2.3, for slowly applied perturbations, the trapped charge will be equal to

$$n_T = n_o \int_0^{\sqrt{2\Phi}} f(0)v dv = n_o \int_0^{\sqrt{2\Phi}} v dv = n_o \Phi \quad (2.31)$$

so, the net charge density in the perturbation region will be

$$n(\Phi) = n_o(1 + \Phi). \quad (2.32)$$

Substituting this into the Poisson equation in cylindrical coordinates gives

$$\frac{1}{r} \frac{\partial}{\partial r} r \frac{\partial \Phi}{\partial r} = \frac{1}{\lambda_D} (1 + \Phi). \quad (2.33)$$

The exact self consistent solution of the potential equation is

$$\Phi(r) = \Phi_o K_o \left( \frac{r}{\lambda_D} \right), \quad (2.34)$$

where  $K_o$  is a modified Bessel function. This solution is known to be the solution to the linearized Debye relation in the limit of small  $\Phi$  [15]. In the case of adiabatic, (or dynamic) shielding, however, it is exact.

In the case of a three dimensional potential, the orbit bending is even more pronounced. In fact, in three dimensions, the perturbation can be shielded even without trapped charge – the density of the particles on untrapped orbits increases as the perturbation potential increases. Following the method of equations 2.26-2.30 it can be shown that for an initial velocity  $v_o$ , the density is

$$\frac{n(r, v_o)}{n_o(v_o)} = \frac{\sqrt{v_o^2 + 2\Phi(r)}}{v_o}. \quad (2.35)$$

To find the response of a plasma to the perturbation, we sum the contributions of each velocity [14]. This gives an untrapped (or “free”) charge density of,

$$\frac{n_F(\Phi(r))}{n_o} = \int_0^\infty \frac{n(r, v_o)}{n_o(v_o)} f(v_o) d^3 v_o = \int_0^\infty \frac{\sqrt{v_o^2 + 2\Phi(r)}}{v_o} f(v_o) d^3 v_o \quad (2.36)$$

Since  $n_F$  depends on  $r$  only through  $\Phi$  we can write

$$\frac{n_F(\Phi)}{n_o} = \int_0^\infty \frac{\sqrt{v_o^2 + 2\Phi}}{v_o} f(v_o) d^3 v_o = \exp(\Phi) \operatorname{erfc}(\sqrt{\Phi}) + 2\sqrt{\Phi/\pi} \quad (2.37)$$

if we assume that the plasma is Maxwellian at infinity. We then add the contribution of the trapped charge, as before,

$$\frac{n_T(\Phi)}{n_o} = \int_0^{\sqrt{2\Phi}} f(0) d^3 v = \frac{4}{3\sqrt{\pi}} (\Phi)^{3/2}. \quad (2.38)$$

Though this trapped charge is unimportant for small values of  $\Phi$  it becomes the dominant contribution when  $\Phi > 2$ . The total charge is therefore

$$\frac{n(\Phi)}{n_o} = \exp(\Phi) \operatorname{erfc}(\sqrt{\Phi}) + 2\sqrt{\Phi/\pi} + \frac{4}{3\sqrt{\pi}} (\Phi)^{3/2}. \quad (2.39)$$

Unlike the two dimensional case, the self consistent solution must be computed numerically. As in the two dimensional case the adiabatic solution differs from the equilibrium case only in the non-linear limit.

## 2.5 One Dimensional Plasmas of Finite Length

The results of the previous sections have all required the assumption that the perturbation does not affect the velocity distribution function of the bulk plasma. This is true in the case of an infinite length plasma, but in some situations, including the experiments discussed in Chapter 3, the plasma has a finite length. This implies that the distribution function of the plasma particles both inside and outside the perturbation can be substantially modified by its presence. We must therefore examine both parts of the orbit.

As in Section 2.3, we will assume that the perturbation is applied slowly on the time scale of the orbital motion of the particles, which, in the one dimensional case, is simply the bounce time. If this is the case, the total action of the orbit,

$$J = \oint v_z dz \quad (2.40)$$

is an adiabatic invariant. This means that we can use  $J$  to label the orbits in a manner that is independent of the depth of the well, and therefore independent of time. Consequently, if the particle distribution can be written in terms of  $J$  it will be independent of the well depth.

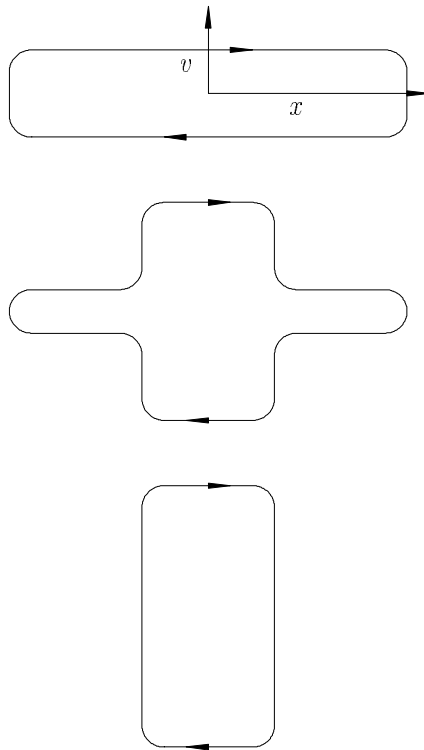


Figure 2.3: The deformation of a phase space orbit with increasing perturbation strength. The perturbation is increasing from top to bottom. Note that the total phase space area of the orbit is conserved.

For simplicity, we will assume that the perturbation forms a square well. The particle phase space orbit will deform as shown in Figure 2.3. Given a particle with unperturbed velocity  $v_o$ , the invariance of  $J$  implies that

$$v_o = \ell v_{in} + (1 - \ell)v_{out} \quad (2.41)$$

where  $v_{in}$  is the particle velocity inside the well,  $v_{out}$  is the particle velocity outside the well and  $\ell = L_{well}/L_{tot}$  is the fractional size of the perturbation. Note that since  $v_o$  is defined to be the particle velocity before the well is applied, it is also a label for the orbits which does not depend on the well depth. Therefore if the initial distribution function  $f_o(v_o)$  is known, Equation 2.41 can be used to find the distribution function in terms of the well depth if a relation between  $v_{in}$  and  $v_{out}$  can be found. Since the well depth changes very slowly on an orbital time scale, energy is conserved on a single orbit,  $v_{in}$  and  $v_{out}$  are related by

$$v_{out}^2 = v_{in}^2 - 2\Phi \quad (2.42)$$

we can now use equations 2.41 and 2.42 to find the velocities after the perturbation is applied in terms of the velocity before the perturbation is applied and the size of the perturbation,  $v_o = v_o(v_{in(out)}, \Phi)$ . Since  $v_o$  does not depend on well depth, we can find the distribution functions after the perturbation is applied in terms of the distribution function before the perturbation is applied,

$$f_{in(out)}(v_{in(out)}) = f_o(v_o(v_{in(out)}, \Phi)) \quad (2.43)$$

As in Section 2.2 this does not take into account the trapped orbits. The bounce action formalism allows this to be calculated as well. As the potential well deepens, the bounce invariant requires that the particles outside the well lose energy. Equations 2.41 and 2.42 imply that

$$v_o = \ell (v_{out} + 2\Phi)^{1/2} + (1 - \ell)v_{out}. \quad (2.44)$$

It is clear from the above equation that when  $\Phi = v_o^2/2\ell^2$ ,  $v_{out} = 0$  and thus the particle will be trapped. At the instant of trapping, Equation 2.41 implies that  $v_o = \ell v_{in}$ . Since the orbit populations do not change after they have been trapped, this will remain true after trapping. The distribution function is

$$f_o \left( \ell (v_{out} + 2\Phi)^{1/2} + (1 - \ell)v_{out} \right) \quad (2.45)$$

outside the perturbation region, and

$$f_o(v_{in}) \text{ for } v_{in} \leq \sqrt{2\Phi} \quad (2.46)$$

$$f_o\left(\ell v_{in} + (1-\ell)\left(v_{in}^2 - 2\Phi\right)^{1/2}\right) \text{ for } v_{in} > \sqrt{2\Phi} \quad (2.47)$$

inside the perturbation region and is shown in Figure 2.4

The particle densities can be found by integrating this distribution function. For a Maxwellian initial distribution, the trapped charge can be found analytically:

$$n_T(\Phi) = \frac{1}{1-\ell} \text{erf}\left((1-\ell)\sqrt{\Phi}\right) \quad (2.48)$$

but the passing charge density and the density outside the well must be found numerically. Once the densities have been obtained as a function of  $\Phi$  a self consistent solution can be found.

The problem of a negative potential (a potential hill) is essentially the same as the problem of a positive potential. The regions inside and outside the perturbation are simply exchanged, the potential is inverted and the problem solved by the methods above. This is possible because the zero of potential is arbitrary, so in a finite plasma, a potential hill is exactly equivalent to a potential well in the region excluded by the perturbation.

## 2.6 One Dimensional Plasmas of Finite Radius

One key assumption that went into the derivation of the self consistent equation for the potential (Equation 2.17) is that the perturbation takes the form of a plane charge. However, our trap, though it may have strong magnetic fields, and thus one dimensional behavior, has a finite size in the direction perpendicular to the magnetic field. The ideas on one dimensional particle trapping presented above can be easily modified to treat this case. The case we will examine is an infinitely long cylindrical plasma of finite radius, confined within a cylindrical conducting boundary. The differences with the infinite case arise mainly in establishing self consistency to the solution. In the case of a finite radius plasma, the exact solution to the Poisson equation becomes complicated by the boundary conditions. We will simplify the problem by making arguments about the form that the solution must take.

Even though the particles are strongly magnetized, and thus tied to field lines, the particles will in general respond differently along field lines at different positions. This

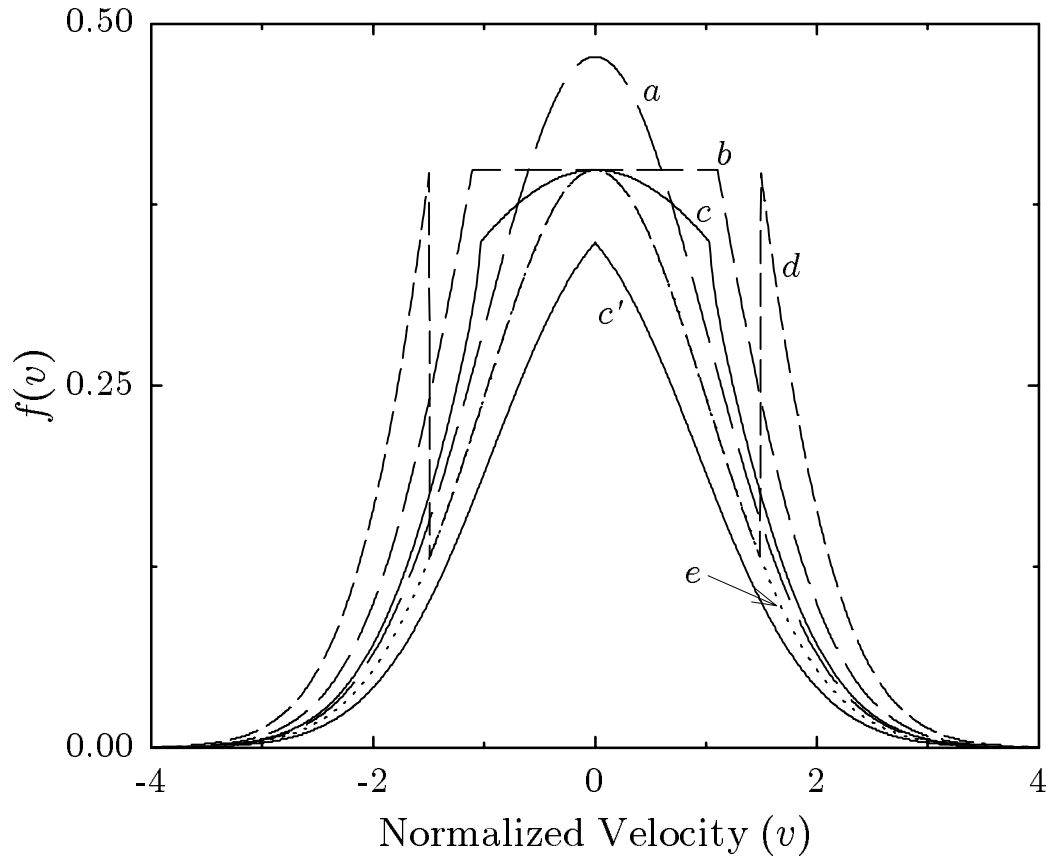


Figure 2.4: Self-consistent distribution functions for an applied well voltage of  $\Phi_w = 2.5$ . Line  $a$  is the Maxwellian distribution for an infinite length plasma, line  $b$  is dynamic distribution function for an infinite length plasma, lines  $c$  and  $c'$  are the dynamic distributions inside and outside the well for the ratio  $\ell = 0.5$ , line  $d$  is the instantaneous distribution for an infinite length plasma, and line  $e$  is the initial Maxwellian distribution before the well is applied (overlaid by line  $d$  for small  $v$ .) Here  $C = 5$  (see Section 2.6) and the shielding efficacies are 0.86, 0.76, 0.79, and 0.56 for lines  $a$ ,  $b$ ,  $c$ , and  $d$  respectively. Note that line  $d$  is likely to be unstable.

would suggest that a higher dimensional model combining the one dimensional response of the particles along field lines with the radial distribution of the field lines would be the most reliable model of the situation. However, in many cases it is sufficient to average over the responses of the different field lines, and assume that all the electrons respond to the same average potential. This model implicitly assumes that the radius of the plasma is much smaller than the radius of the conducting boundary. This potential will have components due both to the external perturbation and to the space charge of the plasma which responds to it,

$$\Phi = \Phi_w + \Delta\Phi_p(\Phi) \quad (2.49)$$

Where  $\Phi_w$  is the external potential well and  $\Delta\Phi_p$  is the difference in space charge potential inside and outside the well region that results from changes in the plasma density, i. e.

$$\Delta\Phi_p(\Phi) = \langle \phi(\Phi, r) - \phi(\Phi_{\Phi_w=0}, r) \rangle_r \quad (2.50)$$

where  $\phi(\Phi, r)$  is the space charge potential of the plasma as a function of both net potential and radius,  $\phi(\Phi_{\Phi_w=0}, r)$  is this quantity when the externally applied potential  $\Phi_w = 0$ , and  $\langle \rangle_r$  denotes an average over spatial position weighted by the plasma density.

Since  $\phi(\Phi, r)$  is a solution of the (linear) Poisson equation,  $\Delta\Phi_p(\Phi)$  must be a linear function of the density,

$$\Delta\Phi_p(\Phi) = C \left[ \frac{n(\Phi)}{n_o} - 1 \right] \quad (2.51)$$

where C is a constant which is equal to the weighted average of the space charge potential of the plasma before the perturbation is applied:

$$C = \frac{\int_0^{R_{boundary}} n(r)\phi(\Phi_{\Phi_w=0}, r)rdr}{\int_0^{R_{boundary}} n(r)rdr}. \quad (2.52)$$

Note that  $C$  is also a normalized quantity, thus the quantity  $CkT/e$  will have units of volts, and will be equal to the average electrostatic potential that a particle in an unperturbed plasma sees.

The complete self consistent response to the perturbation can now be found by solving Equations 2.49 and 2.51 simultaneously.

As an example of how the self consistent solution might be obtained for a plasma of finite radius, we will solve for it in the linear limit. Recall that in the linear limit, the

equilibrium and adiabatic cases were the same, namely,

$$n(\Phi) = n_o (1 + \Phi) \quad (2.53)$$

Therefore the problem can be easily solved approximately for small  $\Phi$ . Substituting,

$$\Phi \approx \Phi_w + C\Phi. \quad (2.54)$$

Therefore, in the linear limit,

$$\Phi \approx \frac{\Phi_w}{1 + |C|} \quad (2.55)$$

for both the equilibrium and dynamic cases. Since  $C$  is the normalized space charge potential, it can be approximately written

$$C \approx \frac{eV_p}{kT} \quad (2.56)$$

where  $V_p$  is the potential in the center of the unperturbed plasma in the case of a non-neutral plasma. Thus the self consistent solution for  $\Phi$  in the linear limit is

$$\Phi \approx \frac{1}{1 + eV_p/kT}. \quad (2.57)$$

The quantity  $1 - \Phi/\Phi_w$  or “shielding efficacy” is plotted for several different types of self consistent solutions in Figures 2.5 and 2.6. In these diagrams, complete shielding corresponds to a shielding efficacy of one, while negative values correspond to anti-shielding.

The self consistent solution to the case where there is no trapped charge (anti-shielding) deserves some special attention. In this case, we have

$$\Phi = \Phi_w + C \left( \exp(\Phi) \left[ 1 - \operatorname{erf}(\sqrt{\Phi}) \right] - 1 \right). \quad (2.58)$$

To lowest order, this becomes

$$\Phi = \Phi_w + \frac{2|C|}{\pi} \sqrt{\Phi} \quad (2.59)$$

which has two solutions. In the limit  $\Phi_w = 0$  these are the trivial solution,  $\Phi = 0$ , and a self sustaining phase space cavity solution,  $\Phi = 4C^2/\pi^2$ . This occurs when a hole is formed in phase space, i.e. when the trapped orbits in figure 1.1 are unfilled. Such phase space cavities have been observed experimentally [16, 17] and in particle-in-cell simulations [18]. These observations will be discussed further in Chapter 4.

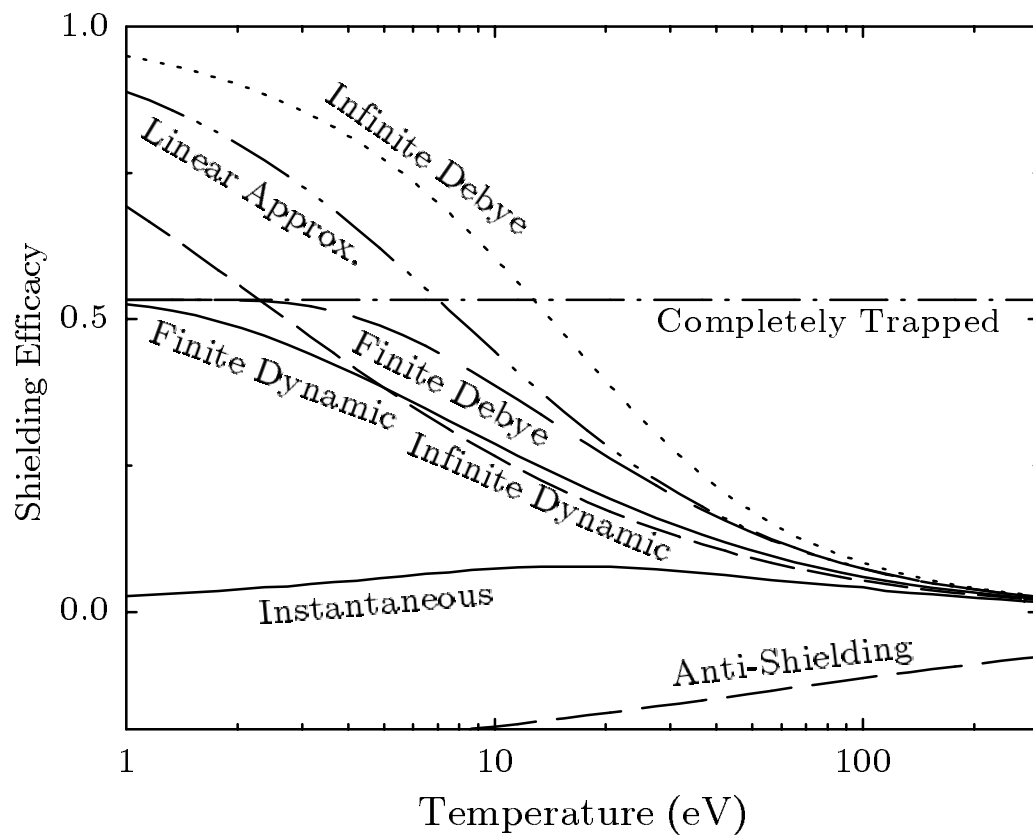


Figure 2.5: “Shielding efficacy”  $1 - \Phi/\Phi_w$  vs. temperature  $T$ , for  $V_w = 30$  V and  $CkT/e = 8$  Volts. Curves are shown for infinite length Debye and dynamic theory, finite length ( $\ell = 0.5$ ) Debye and dynamic theory, the linear approximation, and the case where there is no trapped charge (anti-shielding.)

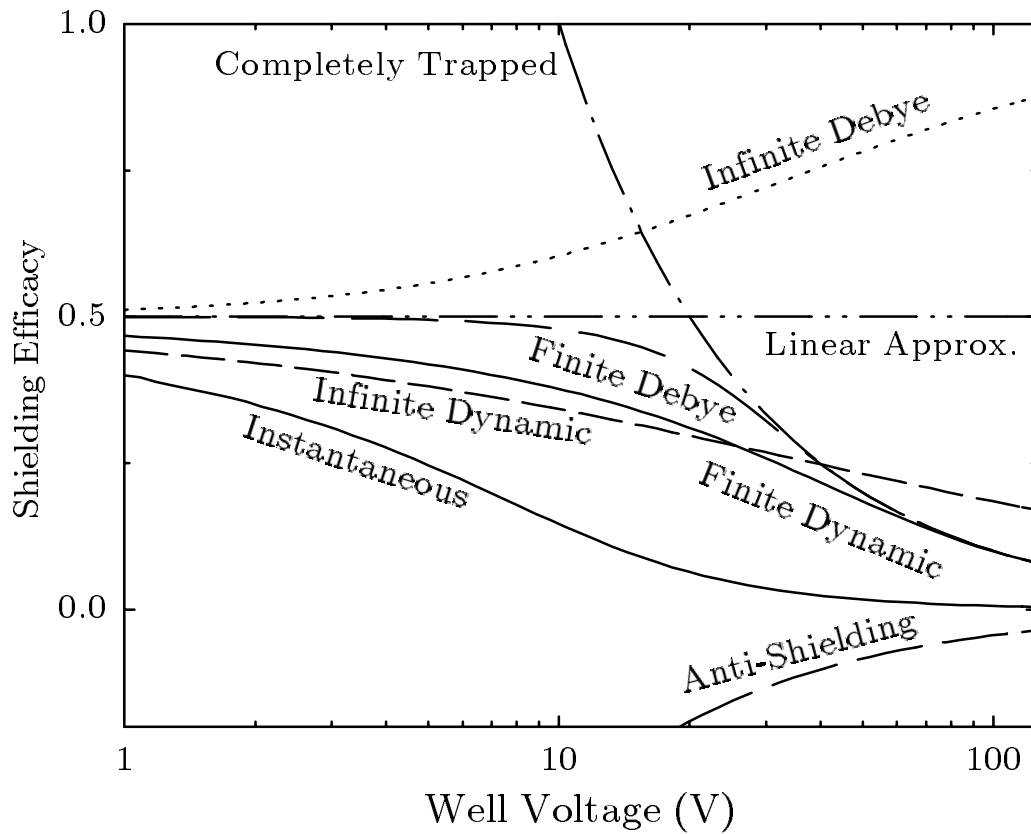


Figure 2.6: “Shielding efficacy”  $1 - \Phi/\Phi_w$  vs. applied well voltage  $V_w$  at  $T = 5$  eV. For tutorial reasons, the density constant  $C$  is given the relatively small value  $C = 1$ . Curves are shown for infinite length Debye and dynamic theory, finite length ( $\ell = 0.5$ ) Debye and dynamic theory, the linear approximation, and anti-shielding. Note that the efficacy decreases in finite length plasmas as the supply of free-electrons is exhausted at large  $V_w$ , and approaches the “Completely Trapped” in the well curve.

## 2.7 Instantaneous Trapping

Previous sections have considered perturbations which occur on collisional time scales and perturbations which occur on time scales which are long compared to the orbital motion of the particles. These types of perturbations are not the only types which can trap particles, however. Particle trapping, and therefore shielding, can also occur for perturbations which are created so quickly that the particles are effectively stationary during the process. We referred to this process earlier as “instantaneous”.

Immediately after such a perturbation, the density in the perturbation region will be unchanged because the particles will not have had time to move. However, the potential energy of these particles will now be different. Some of these particles will now have lost enough energy to become trapped. Those that are not trapped will flow out of the well region and be replaced by particles from the unperturbed plasma. Since the phase space density of the particles on the untrapped orbits is larger outside the well than inside the well, the density of particles will increase somewhat. This mixing is a complicated process and can only be studied numerically. However, some insight can be gained from an analytic treatment based on some simplifying assumptions.

We will begin by assuming that the perturbation forms a square well. Since the perturbation is formed on a time scale which is instantaneous, the phase space distribution function of the trapped particles is unchanged. Therefore, if we assume that the particles are initially Maxwellian, then the distribution of trapped particles will be

$$f(v) = \frac{n_o}{\sqrt{\pi}} \exp\left(\frac{-v^2}{2}\right) \text{ for } v \leq \sqrt{2\Phi} \quad (2.60)$$

immediately after the perturbation is created. Though we have no *a priori* reason to do so, we will assume that there are no other processes which trap charge. Though we can not rule out trapping due to instabilities, there is some evidence from computer simulations [19] that indicates that this assumption is not as problematic as it may seem. We will also assume that the plasma is infinite in length and that the untrapped particles which are initially in the well are completely replaced by particles whose orbits connect to a Maxwellian distribution at infinity. Thus the distribution of untrapped particles will be the same as the distribution in Equation 2.5. Therefore,

$$f(v) = \frac{n_o}{\sqrt{\pi}} \exp\left[-\left(v^2/2 - \Phi\right)\right] \text{ for } v > \sqrt{2\Phi}. \quad (2.61)$$

Note that the completed distribution has a possibly unstable cusp (see Figure 2.4.) Integrating over this distribution gives

$$n(\Phi) = n_o \left( \exp(\Phi) + \operatorname{erf} \left( \sqrt{\Phi} \right) [1 - \exp(\Phi)] \right) = n_o (1 + \Phi + \dots) \quad (2.62)$$

This result can then be used with the Poisson equation for the case of an infinite plane perturbation, or Equation 2.51 for a plasma of finite radius, to find the self consistent response of the plasma to a perturbation.

We see from Equation 2.62 that in the linear limit, the instantaneous shielding result is identical to the adiabatic and equilibrium results. The non-linear response, however, is far weaker; this is illustrated in Figures 2.5 and 2.6. In particular, both dynamic (or adiabatic) and Debye shielding are most effective at low temperature; instantaneous shielding, on the other hand, behaves very differently. To illustrate, we will look at the low temperature limit of Equation 2.62. Since in the previous discussion we have normalized potentials to the temperature, the limit  $T \rightarrow 0$  is equivalent to  $\Phi \rightarrow \infty$ . Using the asymptotic expansion for the error function,

$$\operatorname{erf} \left( \sqrt{\Phi} \right) \simeq 1 - \frac{1}{\sqrt{\pi}} \frac{1}{\sqrt{\Phi}}, \quad (2.63)$$

we find

$$n(\Phi) \simeq n_o \left[ 1 + \frac{1}{\sqrt{\pi}} \frac{1}{\sqrt{\Phi}} \right]. \quad (2.64)$$

The self consistent equation for  $\Phi$  is therefore

$$\Phi = \Phi_w + \frac{C}{\sqrt{\pi}} \frac{1}{\sqrt{\Phi}}. \quad (2.65)$$

Which gives a shielding efficacy

$$1 - \frac{\Phi}{\Phi_w} = \left( \frac{C^2}{\pi \Phi_w^2 \Phi} \right)^{1/2} \approx \frac{|C|}{\sqrt{\pi}} \left( \frac{kT}{\epsilon V_w} \right)^{3/2} \quad (2.66)$$

Therefore, as  $T \rightarrow 0$  instantaneous shielding ceases to have any effect. This is in direct contrast to Dynamic and Debye shielding which work best in this limit. This effect is evident in Figure 2.5. This result must be accepted with some caution, however, as it ignores any instabilities caused by the mixing process or the cusps in the distribution function. These instabilities could dominate the plasma response.

## 2.8 Conclusions

In the sections above, we have shown how the response of a plasma to a perturbation can be calculated for three time scales. We have also shown how the geometry of the plasma and the perturbation will affect the final result. This theory provides us with the ability to calculate the response of a plasma in a wide variety of experimental situations. In particular, the theory of dynamic shielding applies to a wide variety of experiments which were performed on the U.C. Berkeley pure electron plasma trap. This trap, and the reasons why the theories discussed in this chapter apply to experiments performed on it, is discussed in the next chapter.

## Chapter 3

# The Experiment

In order to study the shielding and distribution dynamics of a plasma it is necessary to have a plasma which can be brought into thermal equilibrium, manipulated on time scales both slower and faster than a collision time, that is stable and repeatable, and for which density and velocity distributions can be measured. Pure electron plasmas trapped in a Penning-Malmberg trap satisfy these criteria. In this chapter we will describe Penning-Malmberg traps in general and the U.C. Berkeley pure electron plasma trap in particular. We will also describe the plasma confined in this trap and the diagnostics available to measure its properties. At the end of the chapter we will discuss how the properties of the trap and the plasma make it possible to perform interesting experiments on plasma shielding.

### 3.1 Penning-Malmberg Traps

A Penning-Malmberg trap consists of several (at least three) collimated cylindrical electrodes in a magnetic field parallel to the axis of the cylinders. A schematic of a Penning-Malmberg trap is shown in Figure 3.1. The trapped plasma consists of a single charge species so it can be confined axially by manipulating the voltages on the electrodes. The plasma is confined radially with a strong magnetic field. The Penning-Malmberg trap differs from the well known hyperbolic Penning trap in that the electrodes are cylinders of the same radius as opposed to hyperboloids of revolution. Thus the trap has translational symmetry along the axis of the cylinders, but the vacuum axial potential is not generally harmonic. One example of the axial potential found in a Penning-Malmberg trap is shown in Figure 3.2.

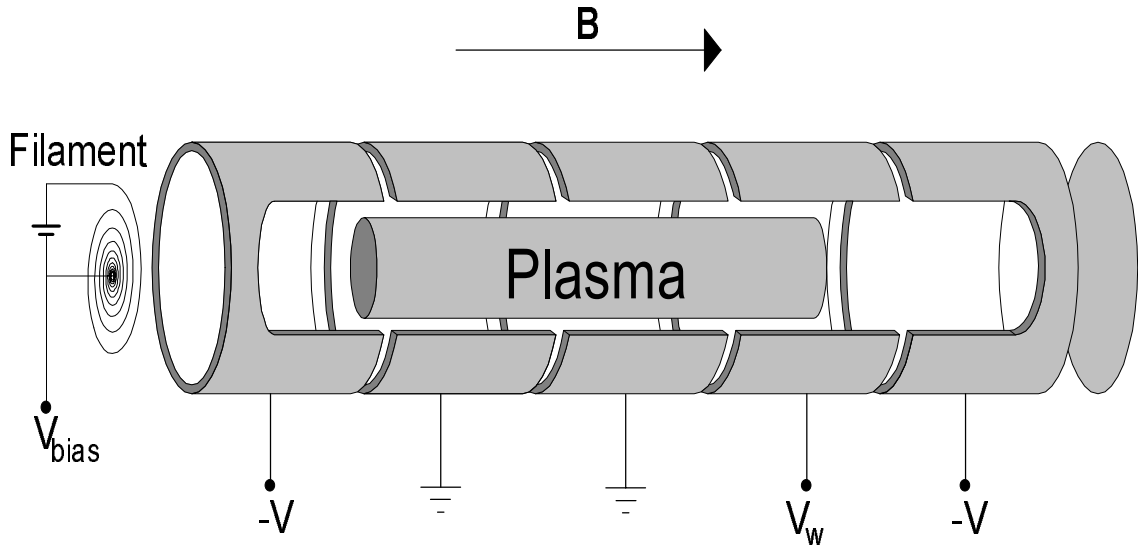


Figure 3.1: Simplified experimental schematic.

The plasmas confined in Penning-Malmberg traps are single species plasmas, and are therefore different from other types of laboratory and space plasmas which are commonly studied. Nevertheless, these plasmas have many interesting properties and much effort has been devoted to their study [20, 21]. One important property of these plasmas is their extremely long lifetime. This is a consequence of a well known angular momentum conservation theorem [22] which states that these plasmas are stable under electron-electron collisions. This implies that these plasmas can come to thermal equilibrium through collisions. Furthermore, since the confinement time is much longer than a collision time, processes can be studied in which the plasma remains in thermal equilibrium throughout the entire experiment.

### 3.2 The U.C. Berkeley Pure Electron Plasma Trap

The U.C. Berkeley electron plasma trap is a Penning-Malmberg trap consisting of nine collimated cylinders of inner radius 1.905 cm. The axial magnetic field can be varied from zero to 2000 gauss. The trap is placed in a vacuum chamber which maintains a pressure of less than  $10^{-10}$  Torr throughout the entire confinement region during the experiment (this includes a measurement of pressure near the filament when the filament is hot.)

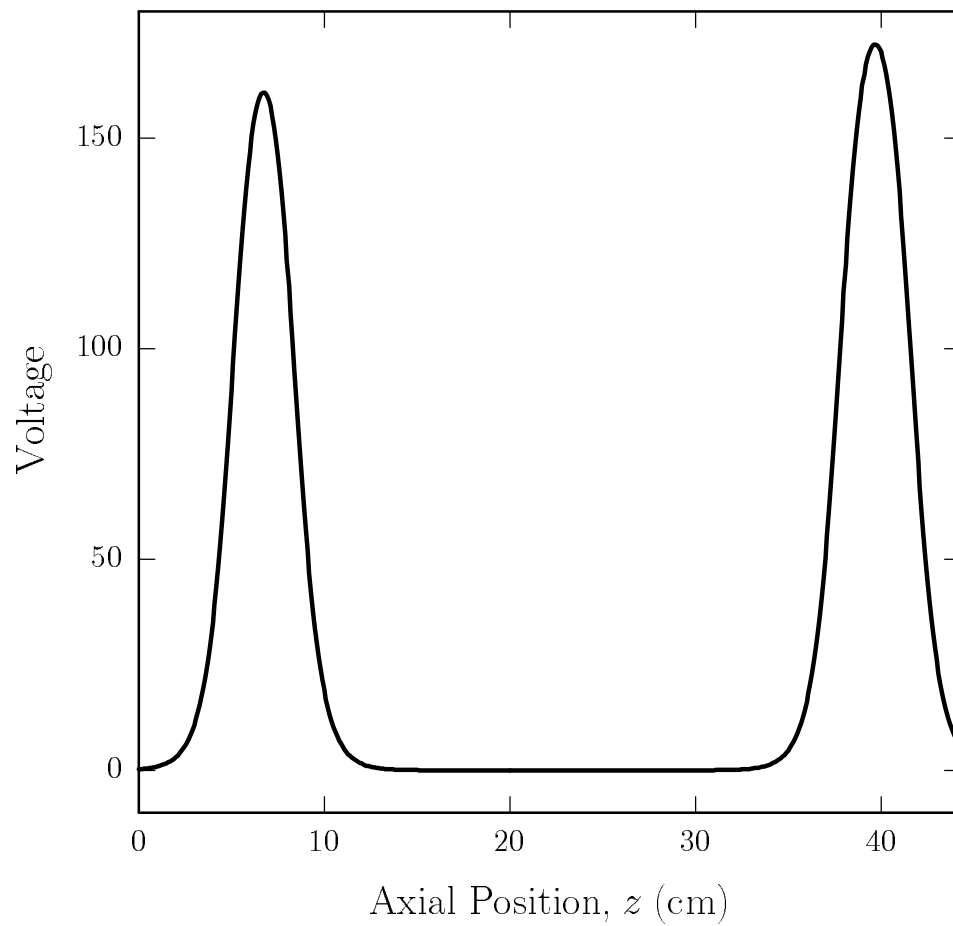


Figure 3.2: The potential along the axis of a Penning-Malmberg trap. The potential shown is for a trap with gate diameter 1.905 cm. and length 44.3 cm. The inject gate extends between  $z = 5.11$  and  $z = 8.36$  while the dump gate extends between  $z = 37.78$  and  $z = 41.62$ .

The electrons are produced by thermionic emission of electrons from a spirally wound tungsten filament. The plane of the spiral is normal to the axis of the trap. This configuration provides a relatively quiescent electron cloud by matching the potential across the face of the filament (due to its own electrical resistance) to the radial potential variation of the electron column that it produces [23, 24, 25]. This is illustrated in Figure 3.3.

A confined plasma is created by allowing electrons to stream from the filament along the magnetic field lines and into the confinement region. The electrons are stopped at the end of the confinement region by a negative electrostatic potential on an electrode which will be referred to as the “dump” gate. The plasma is then pinched off from the filament by applying a negative potential to a gate near the filament which will be referred to as the “inject” gate. This process is illustrated in Figure 3.4. The plasma is now confined between the inject and the dump gates. It can be held in this region for a variable amount of time, then released by lowering the dump gate to ground. This causes the plasma to stream past the dump gate toward a diagnostic region at the far end of the device.

### 3.3 The Plasma

This process of generating and manipulating plasmas allows the exploration of a large range of plasma parameters. Of particular importance is the large range of accessible temperatures. Also, the time scales which are important, such as the bounce time and collision time, are separated by several orders of magnitude. This allows us to examine the plasma in regimes where its behavior is dominated by different processes. Some typical parameters are shown in Table 3.1

### 3.4 Variation of Parameters

The plasma parameters listed in Table 3.1 show a wide variation. To a great extent, this variation is controllable. The next few sections will discuss these parameters and how this control is accomplished. The measurement of these parameters is discussed in Section 3.7.

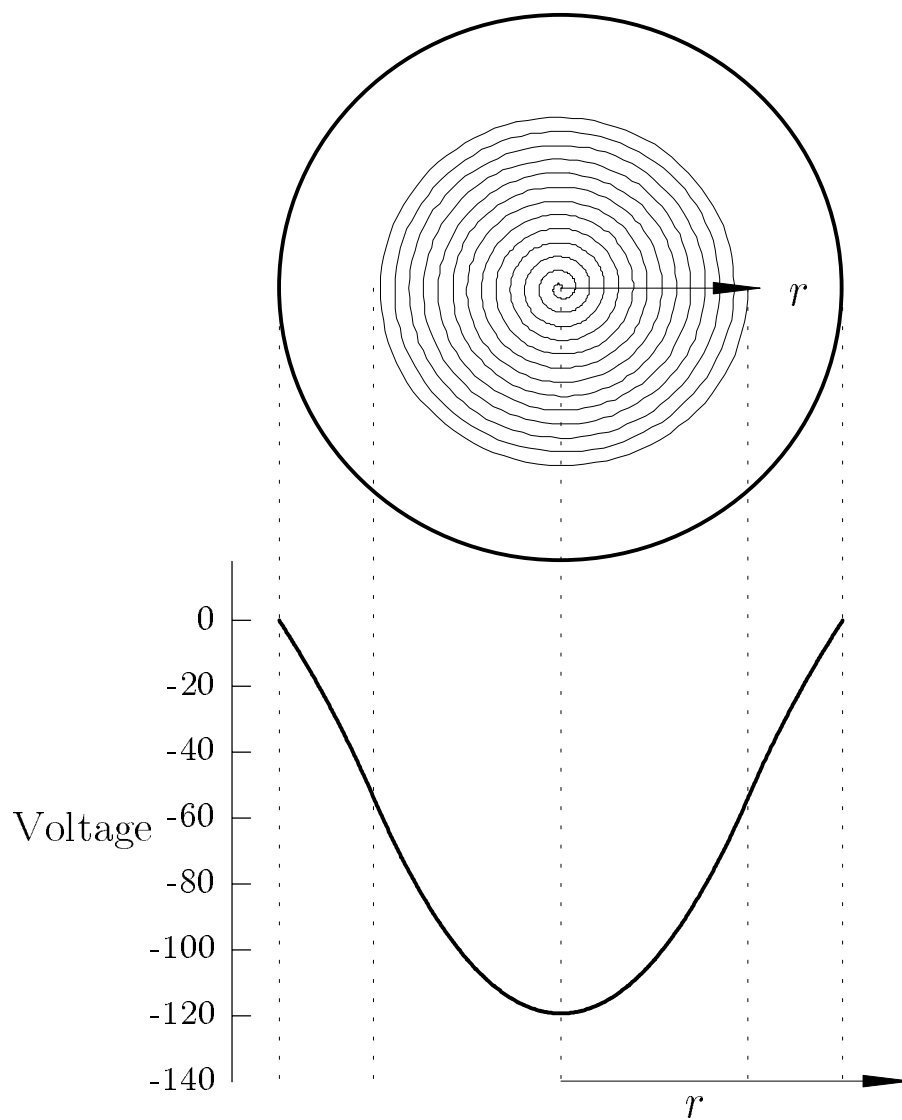


Figure 3.3: The spiral filament and a calculation of one of the potentials that it can produce. Note that the potential increases quadratically from the center to the edge of the filament, then logarithmically to the edge of the trap, which is grounded. (Drawn to approximately 2:1 scale.)

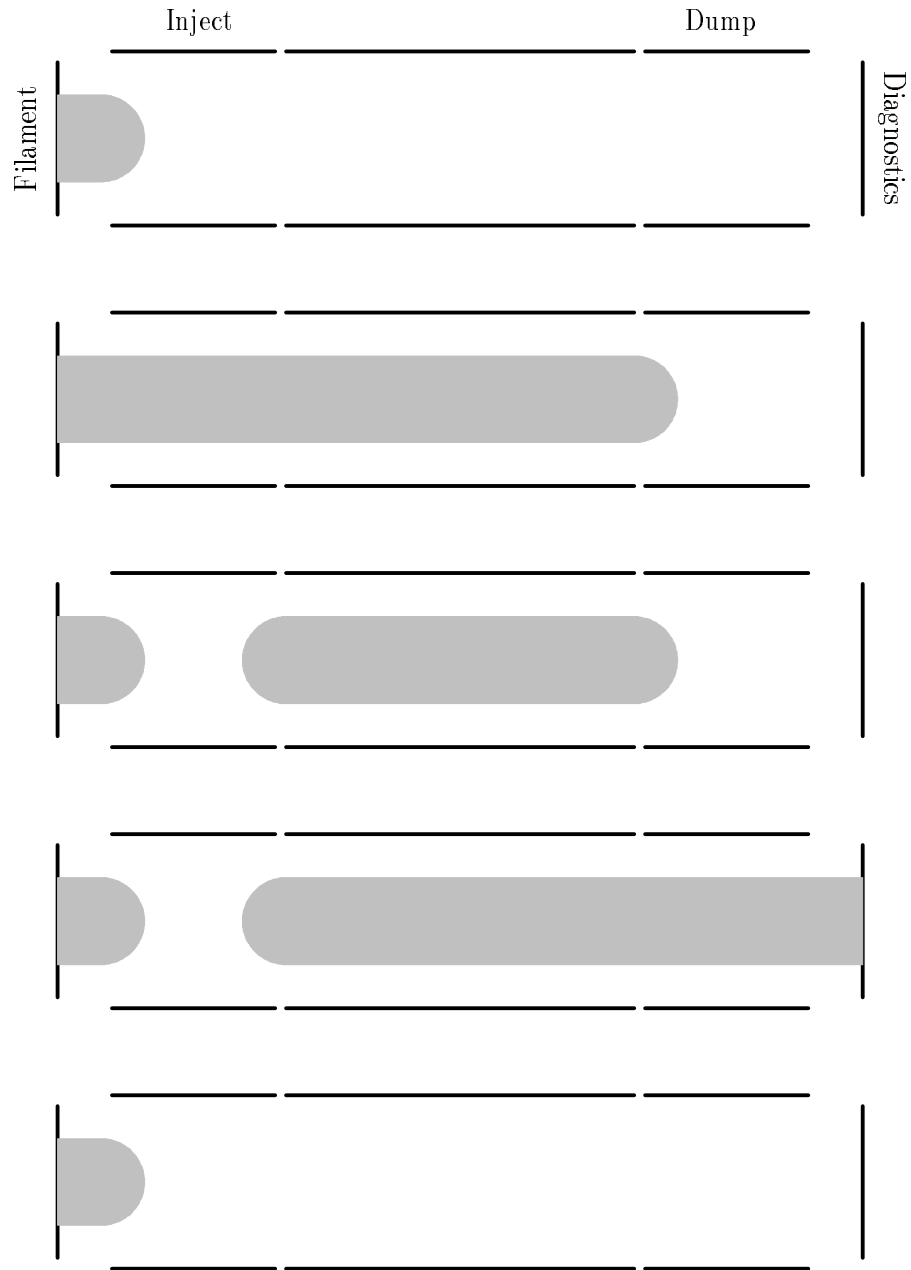


Figure 3.4: The injection and trapping sequence. From top to bottom: 1. The initial state, there are no electrons in the trap, the filament is blocked by the potential on the inject gate. 2. The inject gate is lowered, allowing the plasma to stream in to the trapping region. The inject gate is kept low for many electron bounce times. 3. The inject gate is raised, pinching off the plasma and trapping it. The manipulations that comprise the experiment can now be done. 4. At the conclusion of the experiment, the plasma is dumped to the diagnostic region by lowering the dump gate. 5. After the plasma has been released, we return to the initial state.

Magnetic Field	$B$	500 - 2000 Gauss
Density (Peak)	$n$	$(1 - 4) \times 10^7 \text{cc}^{-1}$
Temperature	$T$	1.3 - 20 eV
Collision Time (e-e)	$\tau_c$	1 - 200 ms
Bounce Time (Average)	$\tau_b$	75 - 500 ns
Plasma Frequency (Peak)	$\omega_p$	30 - 50 MHz
Diocotron Frequency	$\nu_D$	40 - 200 kHz
Cyclotron Frequency	$\omega_c$	0.3 - 6 GHz
Debye Length	$\lambda_D$	0.15 - 1 cm
Larmor Radius	$r_L$	0.8 - 12 mm
Plasma Column Radius	$r_p$	0.7 - 1.3 cm
Plasma Length	$L_p$	20 - 30 cm
Well Length	$L_w$	7 - 11 cm
Space Charge Parameter	$CkT/e$	10 - 20 V

Table 3.1: Typical plasma parameters. See text for the methods by which these are measured or derived.

### 3.4.1 Density

The plasma density coming off of the filament is determined by the filaments voltage profile. This voltage profile is fixed by the filament shape and the voltages at either end. The filament used in these experiments consists of 13 turns of 0.05 mm diameter thoriated tungsten wire, wound in a linear spiral 2.54 cm in diameter. The spiral is maintained by stitching the filament through a thin piece of Alumina ceramic. Though the ceramic provides structural rigidity for the very thin filament wire, it also acts as a significant heat sink. This can cause problems because the heat flow from the filament to the ceramic is different for each stitch. This can cause significant non-uniformities in the filament temperature which can in turn cause significant non-uniformities in density of emitted plasma. To obtain a smooth plasma it is therefore necessary to allow the filament and plasma to come to equilibrium. The linear spiral produces a potential which in equilibrium, matches a uniform density plasma (see Figure 3.3.) In order for the filament to be hot enough to emit electrons, a voltage of 65 Volts had to be applied from center to edge. Therefore, the only parameter that could be varied to affect the plasma density distribution is the bias voltage at the center of the filament. Theoretically, therefore, this filament will produce a uniform density plasma whose radius is determined by the central potential. In actuality, the density is peaked at the center and falls gradually towards the edge of the trap. For most of these experiments, the central potential was held at -40 V. This gave a peak density

of approximately  $3 \times 10^7 \text{cc}^{-1}$ .

### 3.4.2 The Plasma Space Charge Parameter, $C$

The plasma space charge parameter is dependent on both the density of the plasma and the radial distribution of this density. The parameter  $C$  can therefore be varied by altering the filament bias. It can also be varied by changing the preparation of the plasma after it is created. In particular, the means by which the plasma's temperature is changed (which will be discussed in Section 3.4.3) also changes the plasma's radial distribution. Therefore,  $C$  must be measured for each different preparation scheme.

### 3.4.3 Temperature

The initial temperature of the plasma is dependent on the initial conditions, and therefore on the configuration of the filament. After the plasma is created, it can be heated. To heat the plasma, we apply a broad band (3db points at  $\approx 100$  Hz and  $\approx 6$  MHz) noise signal of variable amplitude to the inject gate. This is applied during the plasma preparation process. To ensure that the heating process changes as few other parameters as possible, it is important to ensure that for a given set of experiments, the heating process always takes the same amount of time. The noise signal is generated by a Stanford Research Systems DS345 Synthesized Function Generator. The heating signal lasts for 150 ms at an amplitude which varies for zero to four volts (peak to peak). The signal is coupled to the inject gate via the network shown in Figure 3.5. This was designed to protect the noise source from the high voltage pulser while still efficiently coupling a broad spectrum of noise to the plasma. After heating, the plasma is allowed to equilibrate for 400 ms. This is longer than a collision time and is sufficient to bring the plasma to thermal equilibrium. The final temperature of the plasma as a function of noise amplitude is shown in Figure 3.6.

### 3.4.4 Collision Time and Bounce Time

The collision and bounce times are quantities which are derived from the plasma temperature and density. It is nevertheless important to keep these quantities within the range of applicability of the theory discussed in Chapter 2. For the range of temperatures and densities in these experiments, the collision time varies from 1 to 200 ns. The bounce time varies from 75 to 500 ns.

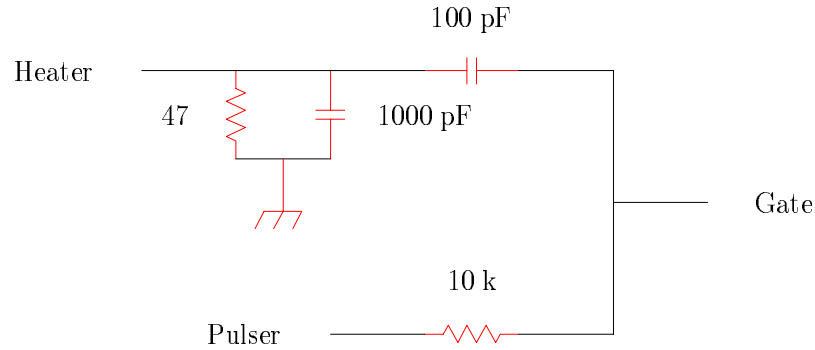


Figure 3.5: The network used to couple the heating signal to the inject gate.

### 3.5 Perturbation of the Plasma

In addition to the standard inject – hold – dump sequence, more complicated axial manipulation sequences were used to study the axial dynamics of the plasma. These include splitting a confined plasma into two pieces, compressing or expanding a plasma, and allowing a plasma confined in one region of the trap to free stream to another region. This flexibility is exploited during the experiments on the plasma’s axial dynamics.

All of these axial manipulations are carried out by changing the voltages on the cylindrical gate electrodes. This experimental tool has several effects and several consequent limitations.

The potential due to an applied voltage in a cylinder in a vacuum can be easily calculated. The form of the potential depends on the ratio of the cylinder’s length to its diameter. Some illustrations of these potentials are shown in Figure 3.7. Any perturbation or manipulation of our plasma using the cylinder biasing technique must therefore be a superposition of these potentials. Though limited in this fashion, these perturbations are adequate for the purposes of these experiments.

These potentials are applied via a length of coaxial cable which passes through the vacuum chamber wall and is connected to a high speed pulser. Theoretically, the speed of the perturbation is limited by the fundamental electromagnetic mode of the confinement region since the excitation of waveguide modes in the trap might produce more complicated perturbations. In practice, however, the speed is limited by the connection from the cable to the gate. For these experiments this was limited to a few microseconds. Future experiments will lower this considerably. A system to lower this to 5 - 20 ns is now being tested. The

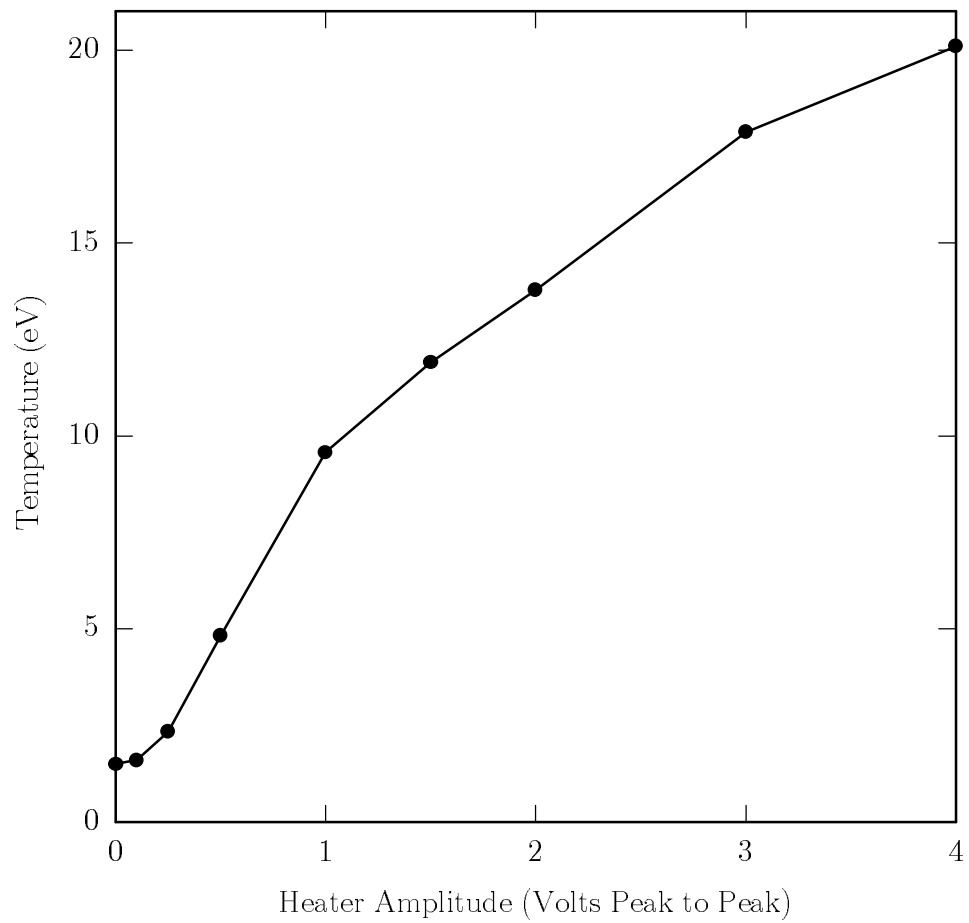


Figure 3.6: The final temperature of the plasma as a function of heating signal amplitude. Error bars are approximately the same size as the plot symbols.

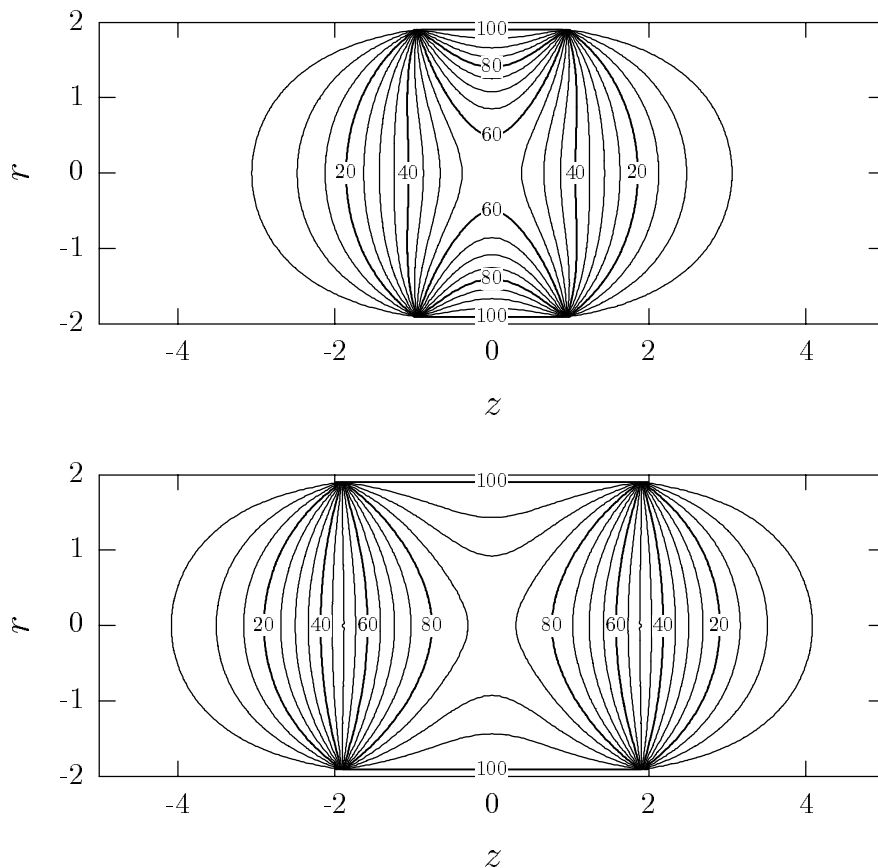


Figure 3.7: Calculated vacuum potentials for a single cylinder in a Penning-Malmberg trap for two different cylinder aspect ratios. We assume that the trap is infinitely long and that all other cylinders are grounded. The calculation was done with a Bessel function expansion. In each case the voltage applied to the cylinder is 100 Volts. The potentials are plotted as a function of radial and axial position. In the top figure the cylinder length is equal to half its diameter (aspect ratio: 0.5.) In the bottom figure, the cylinder length is equal to its diameter (aspect ratio: 1.0.) We assume in each case that the cylinder has radius 1.905 cm.

new system will be limited only by the capacitance of the cylinder and the impedance of the cable.

### 3.6 Diagnostics

The U.C. Berkeley electron trap has three main diagnostics available. These allow a measurement of the total charge in the plasma (i.e. the total number of electrons,) the radial distribution of the charge, integrated over the length of the plasma, and some information about the axial distribution of charge as a function of time.

Total charge and the radial distribution of charge are measured using a flat electrode of known capacitance to ground placed behind a movable pinhole. This consists of a copper and beryllium copper wheel with two small holes of diameter 0.1905 cm and 0.381 cm on opposite sides. The center of the wheel and the position of the holes are arranged in such a way that the pinholes can pass from the center of the trap to the edge when the wheel is rotated. The wheel is mounted on a shaft which is connected to a mechanical rotary feedthrough. It can be turned by a stepper motor mounted outside the vacuum chamber. Since a correspondence between the rotational angle and the radial position of the of the pinhole can be established from geometry, a radial profile of the plasma can be found by using the pinhole to sample the plasma at various radial positions. An example of such a radial profile is shown in Figure 3.8. The charge passing through the pinhole is collected on a copper plate located behind the wheel. This plate is biased to a voltage sufficient to capture the electrons, and is A.C. coupled to a low noise amplifier. This amplifier has a gain of 9.44 and the capacitance of the combination of the plate and the amplifier front end to ground is 440 pF. The resulting voltage can easily be measured with an analog to digital converter and converted to charge with the formula

$$Q = \frac{CV}{g} = V \frac{440 \times 10^{-12}}{9.44} \quad (3.1)$$

Where  $C$  is the capacitance,  $g$  is the amplifier gain, and  $V$  is the measured voltage. The capacitance to ground of the wheel through which the pinhole is drilled is 535 pF . Thus the charge falling on the wheel itself can also be measured by A.C. coupling it to an amplifier. A diagram of these electrodes is shown in Figure 3.9. The electrons follow the magnetic field lines through the pinhole and fall on the plate. Moving the pinhole allows the radial distribution of the axially integrated charge to be measured. The charge which does not

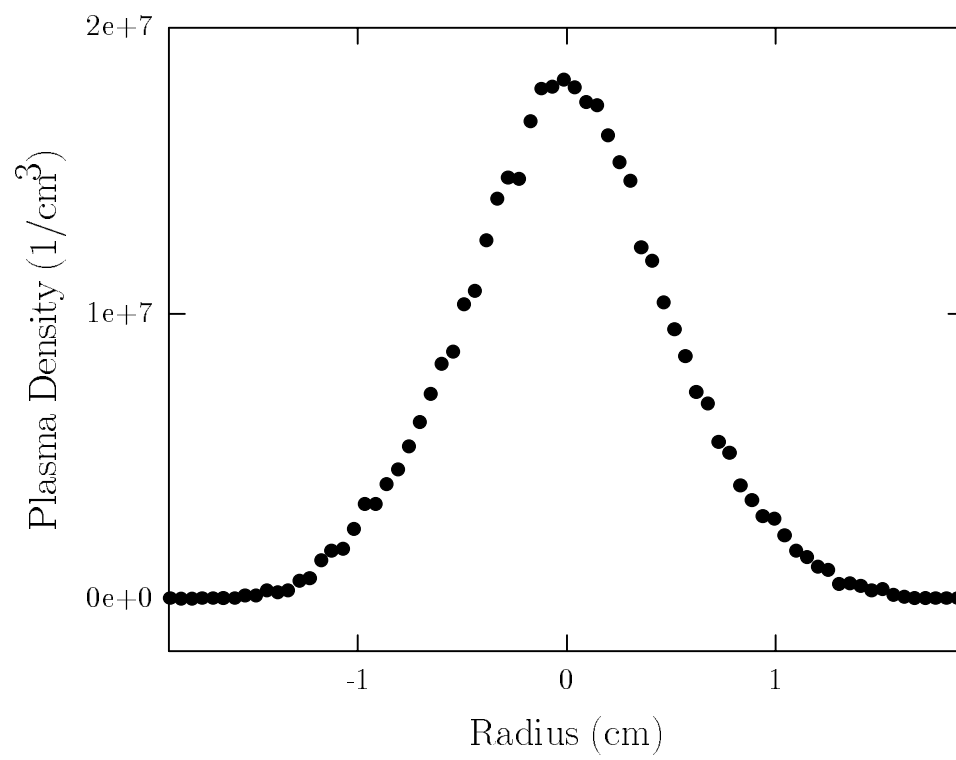


Figure 3.8: An example of the plasma radial profile. Error bars are approximately the same size as the plot symbols.

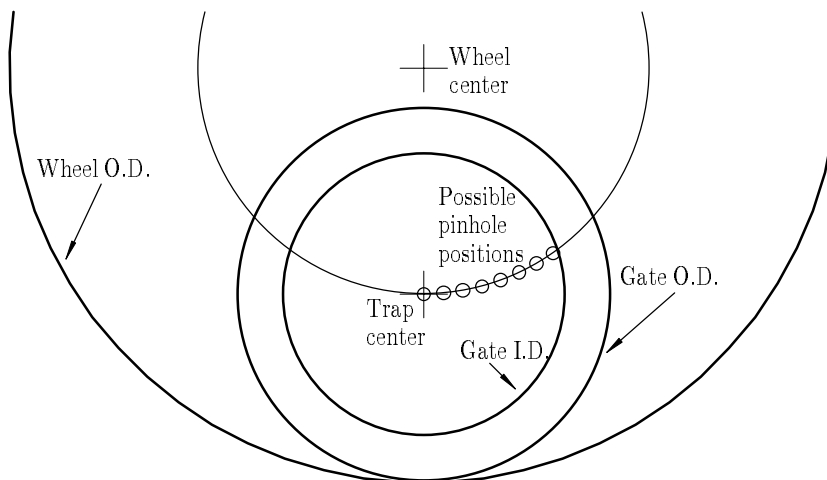


Figure 3.9: The wheel and pinhole diagnostic seen end on. Charge inside the gates streams along the magnetic field lines (perpendicular to the page) and passes through the pinhole and is collected on a plate behind the wheel (not shown). By moving the pinhole across the electron column, its density can be determined as a function of radius.

pass through the pinhole can also be measured. The sum of the two is the total charge in the plasma.

The axial distribution of charge can be measured by measuring the surface charge on the cylinders which bound the confinement region which is induced by the presence of charge inside the cylinders (see Figure 3.10.) Their capacitance to ground is also known. Since the induced surface charge is measured instead of the actual charge, the process is non-destructive. Therefore, some information about the axial distribution of charge as a function of time can be gained. The limitations are due to the fact that the gates have a nonzero length ( $\sim 2.0$  cm), so the measurement effectively averages over a significant region, and due to the fact that since this is fundamentally an A.C. measurement, only relatively rapid changes in charge can be measured. This is sufficient for our purposes. There are also some practical considerations which can cause difficulties with this measurement. The most important of these is the coupling between the perturbation signal and the pickup gate. The voltage on the pickup gate will change due to the mutual capacitance of the pickup gate with the electrode on which the perturbation is applied. Since this change occurs at effectively the same time as the response to the perturbation which we are trying to measure, it is necessary to minimize this mutual capacitance as much as possible. This is accomplished by placing the pickup electrode between two grounded gates. These gates effectively shield the

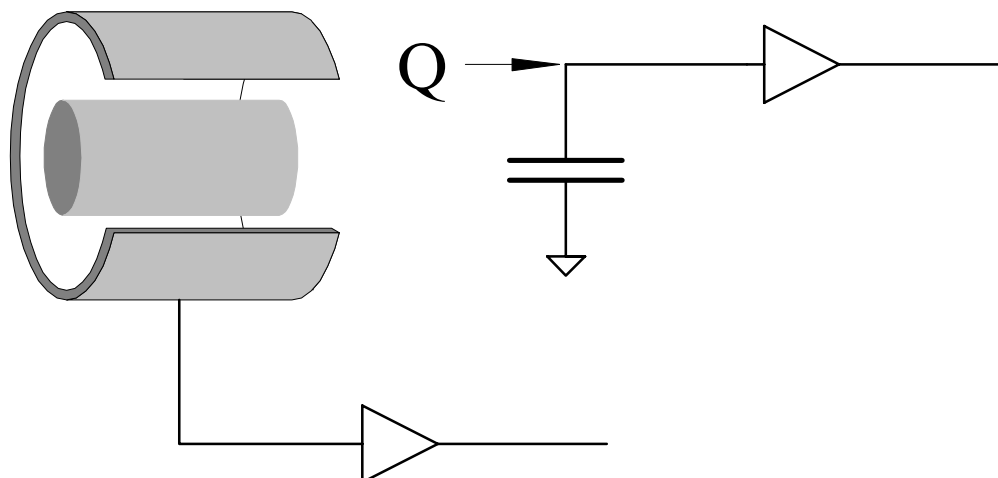


Figure 3.10: Measurement of the axial distribution of charge by using image charge. The basic electrode setup is shown on the left and its equivalent circuit is shown on the right.

pickup electrode from the perturbation electrode. Despite these precautions, the mutual capacitance is still not negligible and the effect of this coupling must be measured for each perturbation created and subtracted from the final result.

## 3.7 Measurement of Parameters

### 3.7.1 Density

The plasma density can be measured in several ways. Most of these methods involve measuring the voltage that all or part of the plasma produces on an electrode with known capacitance and inferring the density. The most straightforward of these is to dump the plasma on the wheel electrode when the pinhole is positioned in such a way that none of the charge passes through. This gives a measurement of total charge from which the average density can be obtained by dividing by the total volume that the plasma occupies. Unfortunately, there is no way to determine the volume *a priori*. Thus this method on its own provides only a guess at the density. It does, however, provide a useful check of other methods by providing an independent measurement of total charge.

The plasma can also be allowed to stream through the movable pinhole. (See Section 3.6 and Figure 3.9.) Since the area of the pinhole is known, and the amount of charge passing through the pinhole can be measured, the only knowledge necessary to

determine the density as a function of position is the length of the plasma. Fortunately, this can usually be calculated [26]. Essentially, though, this measurement gives the integral of density along a given field line, i.e.  $n(r, z)$  averaged over  $z$ .

The lengthwise integrated density can then be compared with a measurement of the total charge in a given longitudinal slice of the plasma by examining the surface charge measurement discussed in Section 3.6 and Figure 3.10. With the total charge in a given length of plasma and a picture of the variation of density with radius, a good estimate of the density profile of the plasma can be obtained. Furthermore, the image charge measurement is non destructive, so a picture of the evolution of the plasma density with time can be obtained.

The method for finding density described above can also be checked by measuring the frequency of the fundamental azimuthal mode of the plasma, known as the “Diocotron” mode. Detailed descriptions of this process can be found in the literature [27, 28, 29].

### 3.7.2 The Plasma Space Charge Parameter, $C$

Once the density distribution has been determined, the space charge potential can be calculated by integrating the Poisson equation. The plasma space charge parameter can then be easily calculated. (See Section 2.6.) Note, however, that since  $C$  is dependent on the preparation scheme, it will vary with temperature. This variation is illustrated in Figure 3.11

### 3.7.3 Temperature

The temperature of the plasma is measured by the dynamic evaporation technique [30]. This method measures the energy distribution of the plasma electrons by slowly lowering the potential on the dump gate and measuring the amount of charge which escapes as a function of that confining potential. Because the amount of charge which escapes is proportional to the integrated energy distribution function, the temperature can be inferred.

The difficulty with this measurement is that in addition to their kinetic energy, the electrons have potential energy from the space charge potential. To reconstruct the entire distribution function it is necessary to completely reconstruct the plasma potential. Since this potential depends on the fraction of the plasma which is trapped, it changes during the measurement process. Therefore, in practice, accounting for this potential energy is

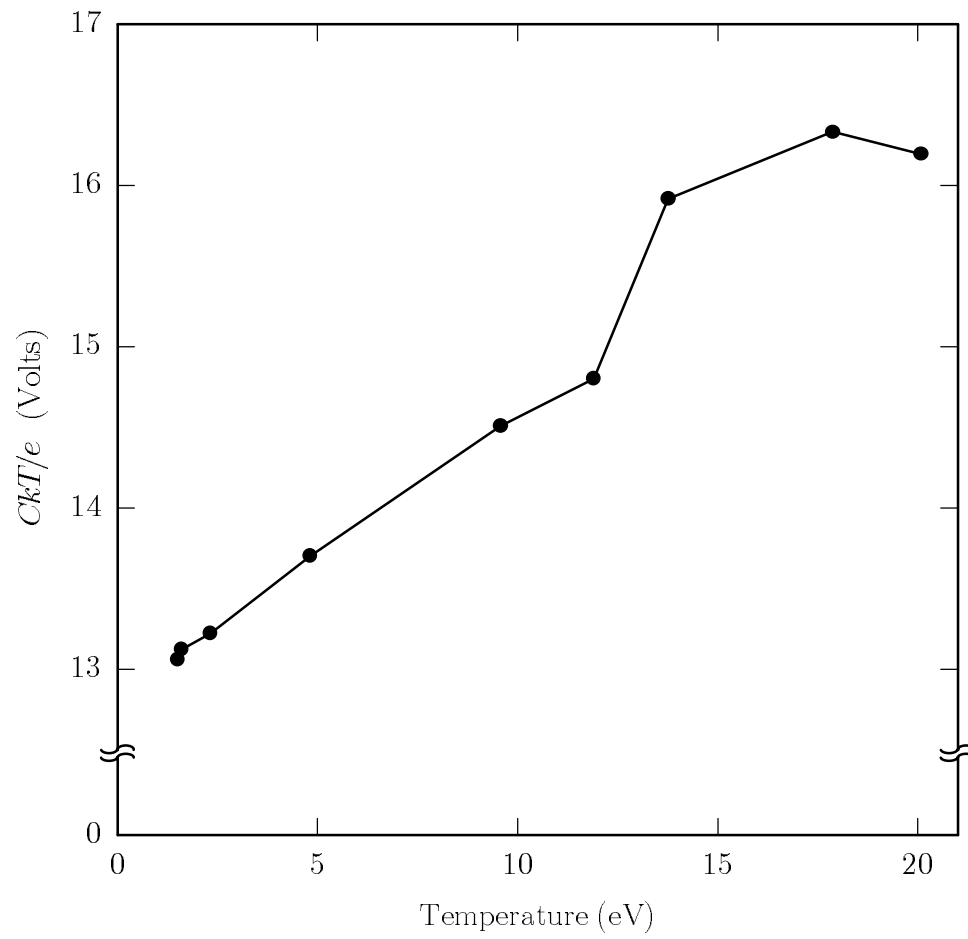


Figure 3.11: The variation of the space charge parameter  $C$  with temperature. The error bars are approximately the same size as the plot symbols.

usually quite difficult. However, if the plasma is in thermal equilibrium, it is not necessary to reconstruct the entire distribution function. The temperature can be inferred from only the most energetic particles, (the tail of the distribution,) and since the plasma potential changes very little when these particles escape (since they represent a small fraction of the total plasma) the effect of the space charge potential can be ignored in this case.

### 3.8 Measurement of the Response to a Perturbation

The response to a perturbation is obtained by measuring the induced change in charge in the perturbation region. This measurement is made using the axial electrode surface charge diagnostic discussed in Section 3.6. We are able to obtain two different pieces of data to describe the response. The most obvious of these is the total charge in the perturbation region. It is also possible to separate the particles which are trapped inside the potential well from those that are not, and to measure the trapped charge (as defined in Section 2.3) independently. This provides an additional measurement which can be used to test the theory discussed in Chapter 2.

### 3.9 Accessible Experiments

There are several features of our device which allow experiments to be done on the dynamics of the distribution function in general and shielding on collisionless time scales in particular. The most important of these features is the separation of the relevant time scales. The important time scales are the collision time and the bounce time. In our case they can be separated by as much as 4 orders of magnitude (see Table 3.1) Because these times are so widely separated, it is possible to isolate dynamic behavior of the plasma that is collisionless, yet adiabatic on bounce time scales. This separation is a fundamental requirement for the validity of the theory discussed in Chapter 2. It is also important to note that since perturbations can be made with axially symmetric electrodes, it is possible to perturb the plasma without exciting radial or azimuthal modes.

Another very important feature of our device is that all of the parameters needed for the theory of collisionless shielding in finite length, finite radial extent plasmas can be measured independently. The theory can be applied without any free parameters, and therefore tested quite rigorously. There is also a fairly wide range of parameter space which

is accessible, especially in temperature and perturbation voltage, which improves the quality of the test.

Finally, the axial surface charge diagnostic discussed in Section 3.6 allows a measurement of several aspects of the response to a perturbation. This measurement can be applied on rapid time scales to measure the effects of collisionless shielding, or slowly to measure the effects of collisional shielding. Therefore we can compare the equilibrium to the non-equilibrium theories in their respective ranges of applicability. The next chapter will discuss the results of several of these experiments.

## Chapter 4

# Results

In prior chapters, we discussed the theory of collisionless trapping. We have also described the U. C. Berkeley pure electron plasma trap and have shown that this trap can be used to test several aspects of the theory. The results of these tests are presented below. We will begin with an experimental comparison of collisional (and therefore thermal equilibrium) shielding and collisionless shielding. This experiment demonstrates that collisional and collisionless shielding are quite different and that there is a need for a separate theory of collisionless shielding. Next we will investigate the relation between trapped charge and shielding and show that a trapping mechanism is in fact necessary for shielding to occur in one dimension. We will also discuss the thermal equilibration of the plasma, and show that in all cases, thermal equilibrium is eventually reached. Finally, we will show direct measurements of the particle distribution functions measured using the dynamic evaporation technique discussed in Section 3.7.3. In all cases, we will show that the experimental results are in agreement with the theory developed in Chapter 2.

### 4.1 Collisional and Collisionless Shielding

It was argued in Chapters 1 and 2 that there is a need for a theory which is based on distribution function dynamics and is therefore distinct from classic Debye shielding. To demonstrate this, we shall compare the behavior of the plasma on collisional and collisionless time scales and see whether there are significant differences. We also compare the dynamic theory of Chapter 2 and the Debye theory with the experimental data in the applicable domains of each.

The experiment was done by creating a series of sets of two identical plasmas. All of the plasmas had a length of 29.4 cm and their temperatures could be varied from 1.2 to 20 eV using the heating process described in Section 3.4.3. For each temperature one of the two plasmas was perturbed on a time scale of 1 ms, (much shorter than a collision time) and the other was perturbed on a time scale of 1 s (much longer than a collision time.) The perturbation was created by biasing some of the cylinders which bound the confinement region. In order to minimize the effect of the gate capacitance on the measurement, a perturbation was created by biasing the cylinders outside the perturbation region with a voltage opposite to the perturbation desired. This is equivalent to applying a perturbation in the perturbation region directly since the zero of potential is arbitrary. Both hill and well type perturbations were created and the perturbations ranged in size from 5 to 80 Volts. For each set of plasma parameters (temperature and perturbation size), there are two data which can be evaluated. These are the total charge in the perturbation region and the total charge trapped by the perturbation. The total charge in the perturbation region for both collisional and collisionless time scales is shown for several values of temperature and well depth in Figure 4.1. Figure 4.1 also shows the dynamic and Debye calculations. All of the plasmas examined were created with the same filament conditions. Despite this, the parameter  $C$  is affected by the heating process and this variation must be accounted for. In the data shown in Figure 4.1,  $CkT/e$  varies from 11.9 V to 16.3 V.

Figure 4.2 shows the trapped charge as a function of temperature and well depth. One important caveat about the data in Figure 4.2 is the fact that the charge that is measured is the charge that remains after the dump gate is lowered. Since the removal of the free charge during the dump changes the space charge potential, and thus the total well depth, the charge remaining trapped after the dump is not the same as the charge trapped in the perturbation before the dump. Since the removal of the space charge causes the well to become shallower, there is in fact less trapped charge after the dump. The effect of this change in well depth can be found by calculating the space charge potential due only to the trapped charge (compare with Equation 2.51.)

$$\Delta\Phi_p(\Phi) = C \left[ \frac{n_T(\Phi)}{n_o} - 1 \right]. \quad (4.1)$$

This expression is used to calculate the total potential (applied plus space charge potential) after the dump in the theoretical calculations shown in Figure 4.2.

This data clearly shows that there are significant differences between thermal equi-

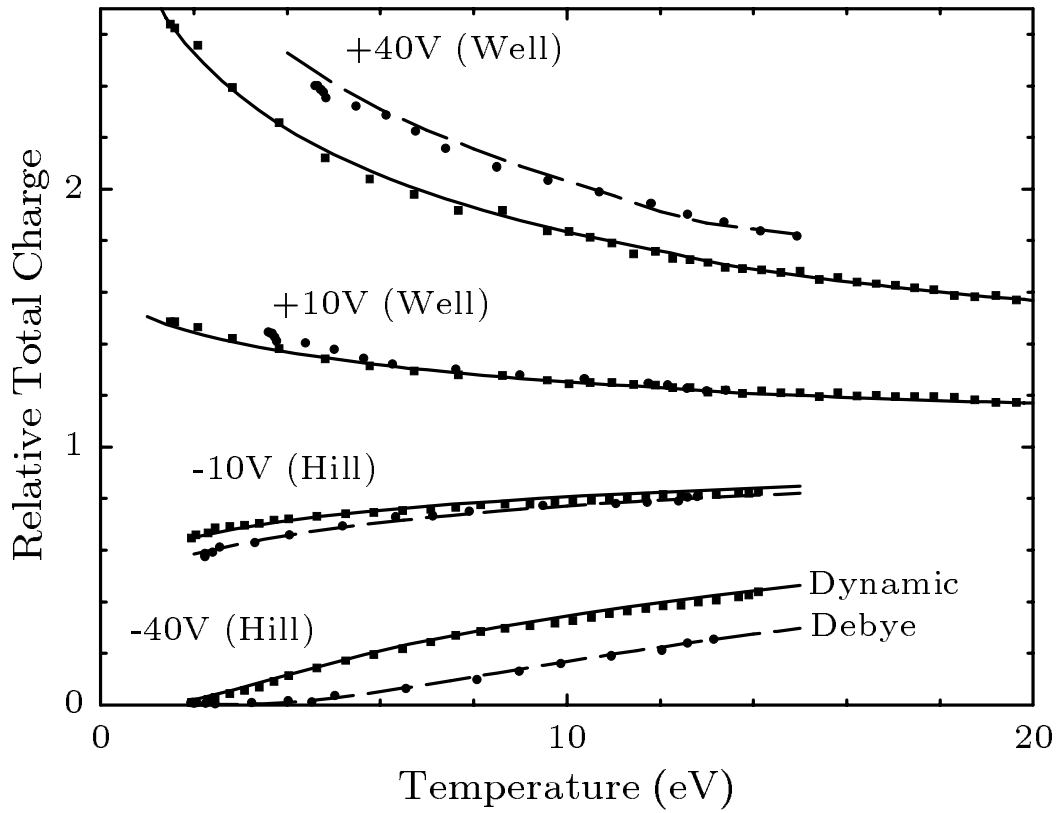


Figure 4.1: Total charge vs. temperature relative to the total charge in the unperturbed plasma. Here  $\ell = 0.27$  for wells and  $\ell = 0.44$  for hills. The measured plasma density varies with temperature such that the density constant  $CkT/e$  varies between 13.0V to 16.3V for wells, and 11.9V to 15.4V for hills. The lines are calculated from the theory described in Chapter 2 using the value of  $C$  measured at each point. More detail on the variation of  $C$  with temperature is given in Section 3.7.2 and Figure 3.11.

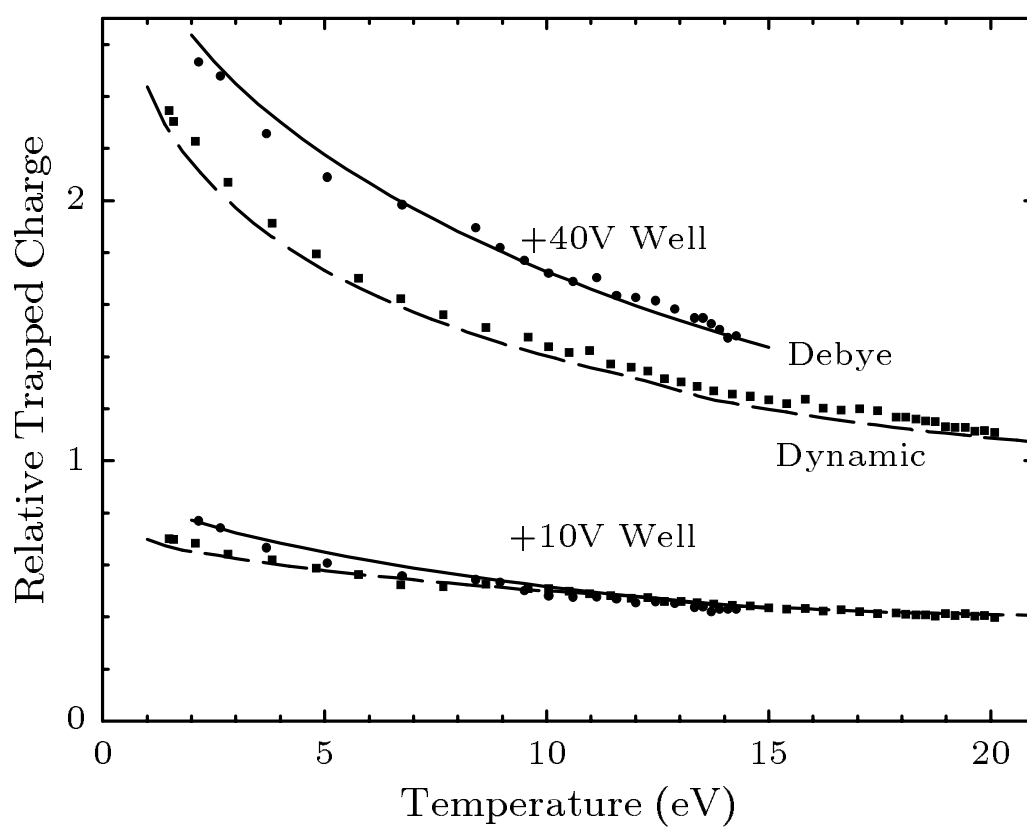


Figure 4.2: Relative trapped charge vs. temperature. Parameters are identical to well parameters in Figure 4.1.

librium and non thermal equilibrium shielding in the nonlinear limit. Figures 4.1 and 4.2 also show that there is excellent agreement between experiment and theory as long as the theory is applied in the appropriate time domain.

## 4.2 The Importance of Trapped Charge – Anti-Shielding

The theories of Chapter 2 are based on the idea that trapped charge is necessary for shielding in one dimension. Furthermore, it was claimed that if there is no trapped charge, a negative perturbation will be anti-shielded.

To test this assertion, it is necessary to create a potential well in such a way that charge can not be trapped. This is done by creating the perturbation before there is plasma present. In order that there be a valid comparison with the case where charge is trapped, we use two similar plasma manipulation schemes. The fundamental design for these two schemes is that they should differ only in that one scheme should trap charge and the other scheme should not. Otherwise they are made as nearly identical as possible. Each scheme proceeds in five steps (see Figure 4.3.) In the case where no charge is to be trapped, the plasma is first injected into a part of the confinement region. Second, the perturbation is formed by creating a potential well in the same manner as described in Section 4.1. Third, the plasma is allowed to flow into the perturbation region. Fourth, the “free” charge is dumped and measured. Fifth, the trapped charge is measured. In the case where charge is to be trapped, the second and third steps are interchanged.

The results of this experiment are shown in Figure 4.4. Several important conclusions may be drawn from these data. One conclusion is that it is possible to create a perturbation in a plasma which, for a brief amount of time (the exact time depends on the perturbation size, but is of order  $1\mu\text{s}$  for a 1 Volt well,) traps little charge. Figure 4.4 does show some trapped charge even in the non-adiabatic case, however. This is due to an instability which grows more rapidly as the perturbation increases in size. Since the data were taken at a fixed time, the net effect of this instability is to cause an increase in the trapped charge which is measured. The exact nature of this instability is unknown, but it may be related to the two stream instability caused by the relative lack of electrons at zero velocity in the perturbation region in the non-adiabatically created test well case. More importantly, we find that when there is no trapped charge, the perturbation is anti-shielded. This is clearly shown by the decrease in total charge up to well depth where instabilities

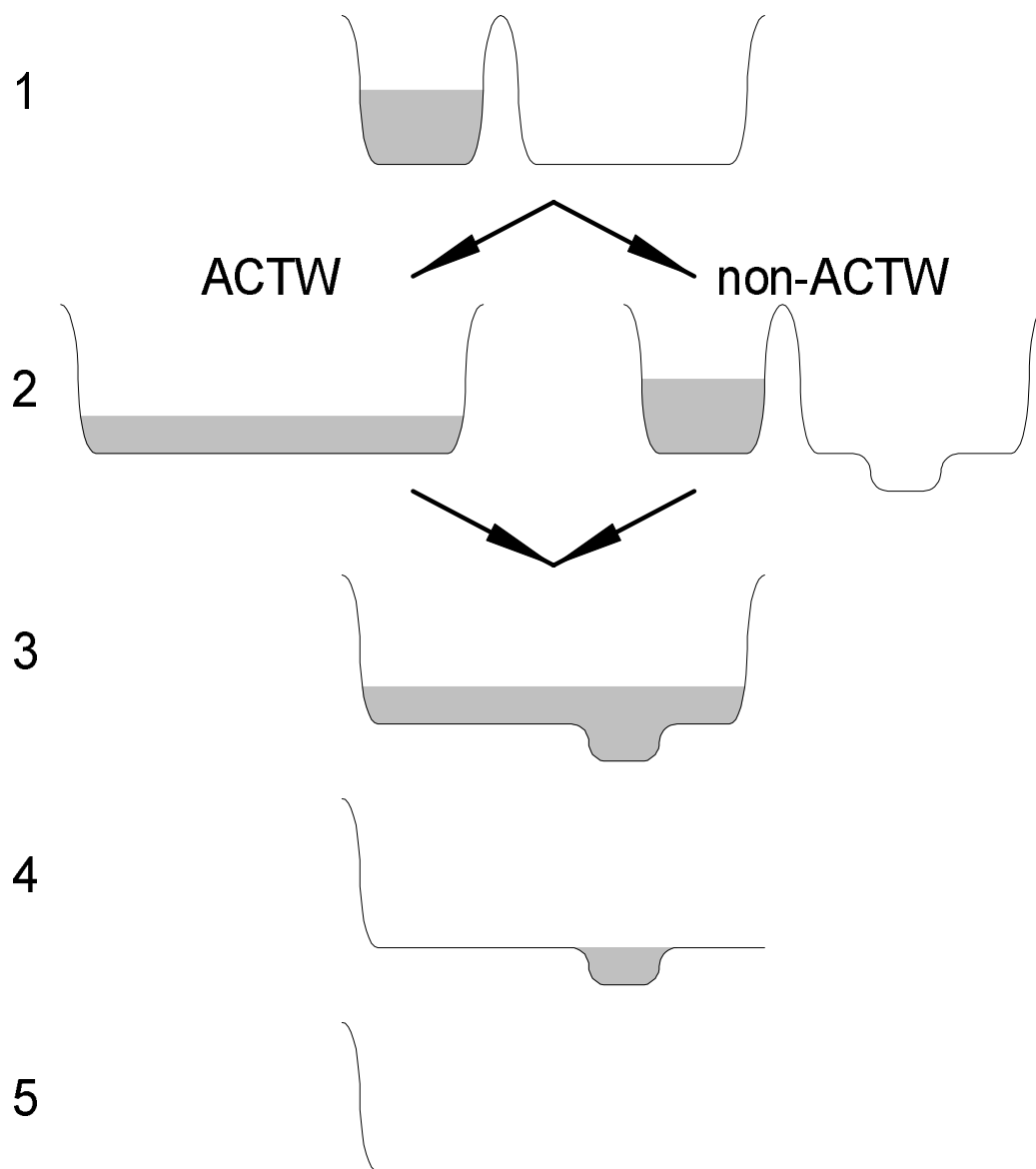


Figure 4.3: Schemes for examining the effect of trapping. The solid line shows the potential energy of an electron as a function of position. The shaded region represents the plasma electrons. In the adiabatically created test well case (shown at left), the well is created with the plasma present. In the non adiabatically created test well case, the well is created before the plasma is let into the confinement region. Thus, no charge is trapped.

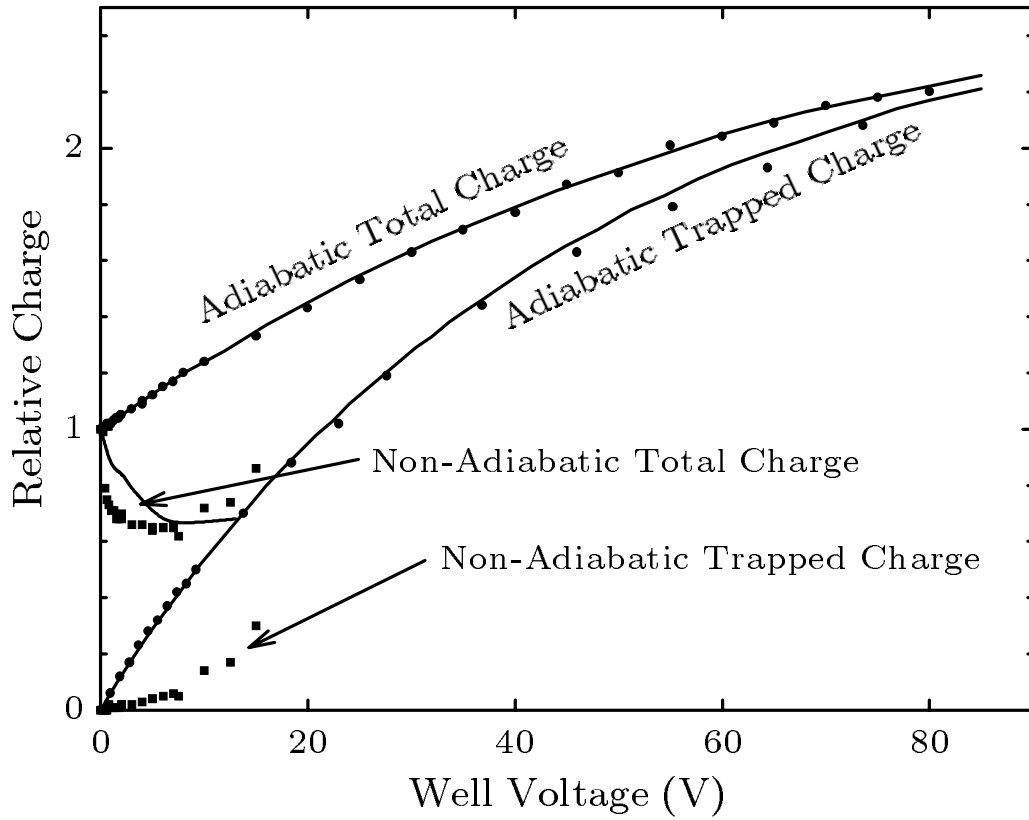


Figure 4.4: Relative charge vs. well voltage. Relative charge is normalized to the charge found when the applied well voltage,  $V_w = 0$ . Here  $\ell = 0.28$ ,  $T = 6.8 \text{ eV}$  and the density scale constant is  $C = 2.29$ . Lines are from the analytic theory given in Chapter 2 for the adiabatic case and from a PIC simulation [31] in the non-adiabatic case.

start to become dominant. Finally, this experiment shows that anti-shielding only occurs when there is no trapped charge, since the plasma prepared in a nearly identical fashion save that charge is trapped shows shielding behavior which is predicted by the dynamic shielding theory of Chapter 2.

In addition to the data shown in Figure 4.4, we also see axial oscillation for very small well depths. These oscillations have an amplitude which is a sizable fraction of the total charge density which implies that they are highly nonlinear. There is some evidence from computer simulations [31] which may indicate that these oscillations are due to the self sustaining phase space cavities which were predicted in Section 2.6.

### 4.3 The Approach to Equilibrium

If a perturbation is created in a time which is much shorter than a collision time, then the plasma may exhibit behavior which is not predicted by thermal equilibrium theory. However, if the plasma is kept for several collision times in the presence of the perturbation, it will eventually come to thermal equilibrium through collisions. This is true of plasmas which initially shielded or anti shielded the perturbation. Experimental data which illustrates this equilibration process is shown in Figure 4.5 and Figure 4.6.

### 4.4 Distribution Functions

Since all of the theories presented earlier to describe plasma shielding of a perturbation are based on the dynamics of the velocity distribution function, it would be very useful to measure these distribution functions directly. This turns out to be a very difficult task, given the diagnostics available.

The distribution function is measured with the dynamic evaporation technique discussed in Section 3.7.3. The primary limiting factors on this technique are the confounding effect of the plasma space charge on the energy distribution and the fact that what is measured is not the distribution function itself, but its energy integral. To minimize the space charge effect, we measured the distribution function of a very tenuous plasma (the space charge parameter  $C = 0.26$ .) Measuring the response of a very tenuous plasma adversely affects the signal to noise ratio however, and since numerical differentiation is problematic

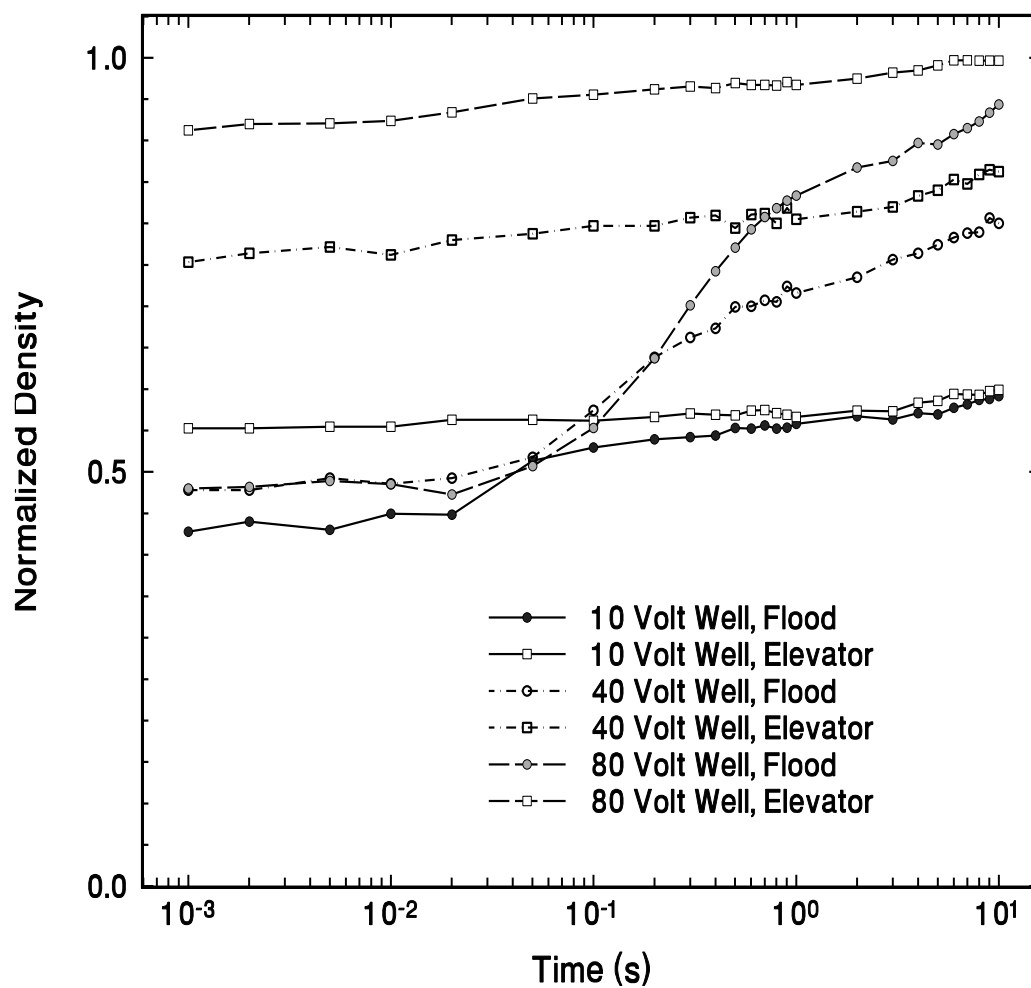


Figure 4.5: The plasma approach to equilibrium due to collisions. This shows trapped charge normalized by total charge as a function of time after the well is created for both adiabatically created (elevator) and non adiabatically created (flood) test wells. The global evolution beyond 10 s is due to radial expansion of the plasma, so there is no data shown in that regime. The differences in trapped charge between the adiabatic and non adiabatic case at 10 s are due to differences in the temperature of the plasma after the well has been created.

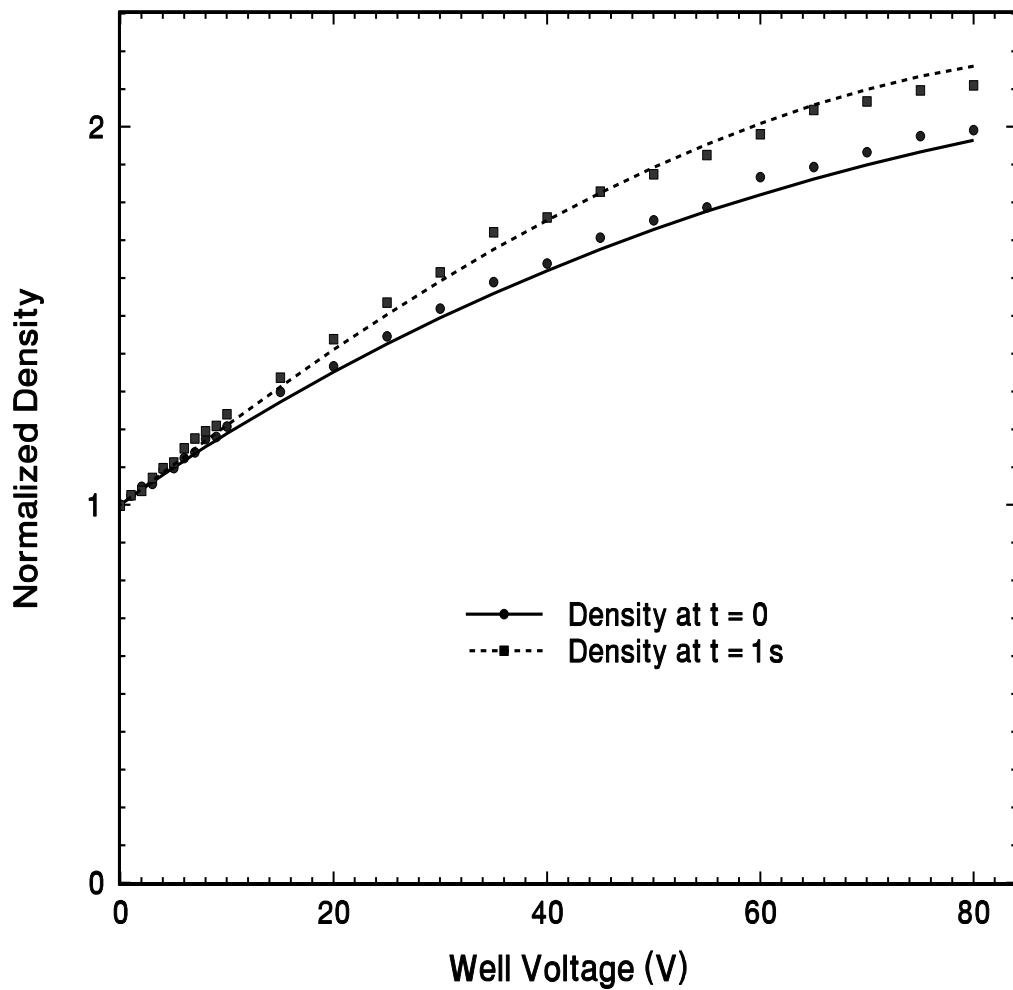


Figure 4.6: Total charge vs. well voltage at two different times. The data is normalized to the density before the well is created. The  $t = 0$  measurements were made immediately after the test well was created, while the  $t = 1$  s measurements were made after the plasma had become equilibrated through collisions, 1 s after the well was created. The lines are calculated from the theory described in Chapter 2

in a noisy environment, we will present only integrated distribution functions:

$$I(E) = \int_0^{\sqrt{E}} f(v)dv. \quad (4.2)$$

Two of these distribution functions are shown in Figure 4.7. This shows how the integrated distribution function changes with the adiabatic application of a perturbation. The significance is that it is no longer Maxwellian, and that it matches the predicted distribution quite well.

## 4.5 Conclusions

The most important conclusion that can be drawn from the data presented in this chapter is that trapped particles are necessary for shielding in one dimension. Without some mechanism for trapping particles, a perturbation in a one dimensional plasma will be enhanced by the space charge potential of the plasma and will therefore be anti-shielded. A second and related conclusion is that on collisionless time scales, collisionless mechanisms must be invoked to explain the response of a plasma to a perturbation. In a collisionless plasma, the concept of thermal equilibrium is not valid, and thus the details of the process by which particles move to trapped orbits must be understood if the shielding behavior of the plasma is to be understood. Finally, one such mechanism, based on adiabatic trapping, and the theory derived from it in Chapter 2 has been shown to explain the response of a non-neutral plasma confined in the U.C. Berkeley pure electron plasma trap under a wide range of conditions.

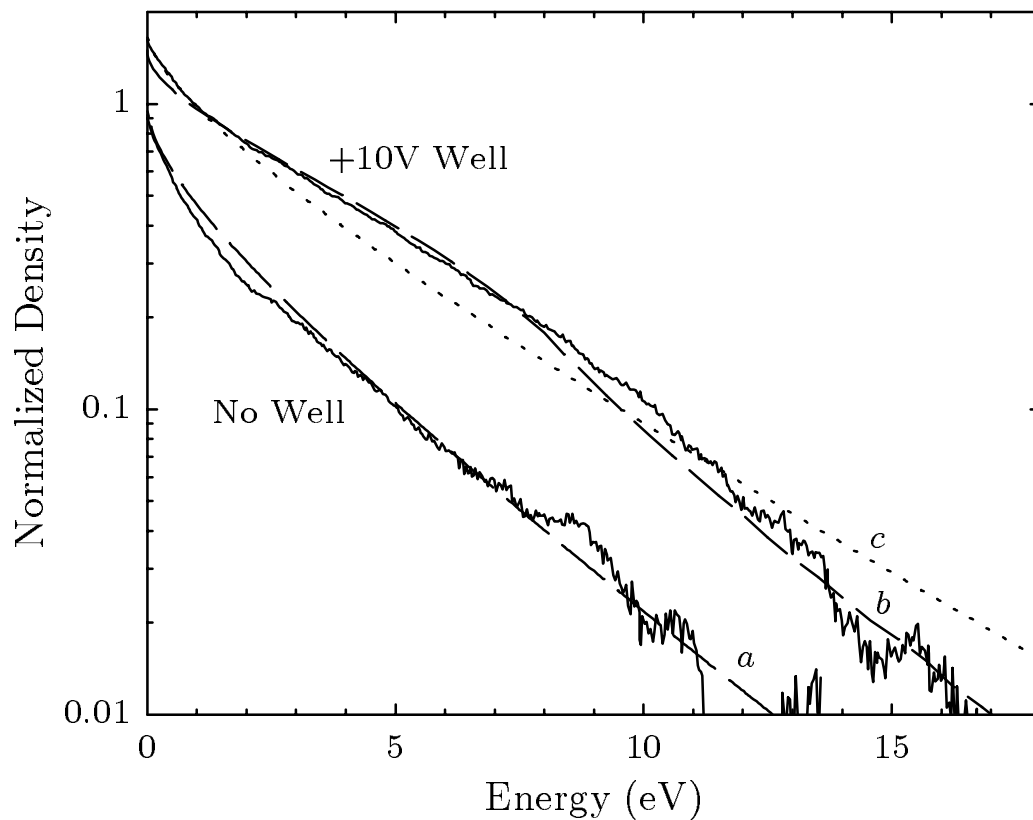


Figure 4.7: Experimental integrated distribution functions,  $I(E)$ . Shown are the experimental data taken using the dynamic evaporation technique (solid lines) before and after the application of a +10 V well, the (a) best fit Maxwellian ( $T = 3.8$  eV) to the initial plasma, the (b) calculated “Dynamic” distribution in the well, and (c) the calculated Maxwellian ( $T = 5.2$  eV) to which the experimental data should relax due to collisions. Here  $\ell = 0.44$ .

## Chapter 5

# Conclusions

During the course of this research, it has become apparent that several new concepts are crucial to the understanding of plasma shielding. These concepts fall into two main categories. The first is the importance of particle trapping to shielding. The second concerns the mechanisms by which trapping, and thus shielding, occurs.

This research has demonstrated that in one dimension, particle trapping is necessary for shielding. Although this trapping can occur due to collisions, we have shown that there are also collisionless trapping mechanisms. Even so, it is possible to create a situation where no charge is trapped. In this case, the phenomenon of anti-shielding will be observed – where the perturbation will be enhanced by the plasma. Results which are valid for one dimensional plasmas are very important since all strongly magnetized plasmas are effectively one dimensional.

In two and three dimensions, a somewhat more complicated situation arises. Here, the simple flux conservation argument used to explain the one dimensional case must be modified to include the curvature of the orbits (see Section 2.4). Nevertheless, trapping is still very important. Previous authors [12] have shown that without trapping in two dimensions, a perturbation will neither be enhanced nor shielded by a perturbation, while the shielding caused by a perturbation in three dimensions will be diminished. We have extended these results to include the effect of collisionless trapping, and shown that shielding occurs in both cases.

Two different collisionless trapping mechanisms have been explored, dynamic (or adiabatic) and instantaneous. Both of these are compared with collisional trapping. The principal difference between collisional and collisionless trapping lies in the fact that the

latter can produce non-Maxwellian distribution functions. The principal problem, theoretically, is therefore finding these distribution functions. We have found that collisional and collisionless shielding differ primarily in the non-linear regime. Dynamic shielding is generally weaker than Debye shielding, and instantaneous shielding is weaker still.

Despite the fact that equilibrium and non-equilibrium results often agree numerically in the linear limit, linearization of the problem presents important theoretical problems. This is due to the fact that the size of the region of phase space where charge is trapped scales as  $\sqrt{\Phi}$ , it is therefore never negligible. The recognition of this fact is not new. It has been used as the basis for the understanding of BGK modes as well as other plasma physics phenomena [32].

The experiments on non-neutral plasmas that we performed not only confirmed the importance of trapping to shielding, they have also confirmed the usefulness of our models of collisionless trapping to explain plasma shielding. This was shown by experiments contrasting situations with and without trapping as well as comparing collisional to collisionless trapping. We also demonstrated some of the changes in the velocity distribution function brought about by collisionless trapping.

## 5.1 Applications

A motivation for these experiments was to examine the possibility of confining a neutral plasma (either electrons and ions or electrons and positrons) in a Penning trap. The plan was to use a “nested well” scheme. This uses two barriers of opposite polarities on either side of the trap. Thus particles of both positive and negative charge can be trapped. This scheme is illustrated in Figure 5.1. A barrier to one species is, however, a well to the other. If all the electrons were to fall into the wells which provide barriers to the ions or positrons, either the charge will separate or the barriers will be screened away. If this well could be anti-shielded, this scheme would be much more feasible. These experiments have shown, however, that even if the perturbation is initially anti-shielded, instabilities will eventually trap charge and shield the perturbation. It may be possible, however, to prevent these instabilities. Some speculation on how this might be accomplished follows.

The key to anti-shielding is preventing charge from being trapped in the perturbation region. If a perturbation can be made that does not trap charge, then it will be anti-shielded. One possible method would be to continuously drive particles out of the well.

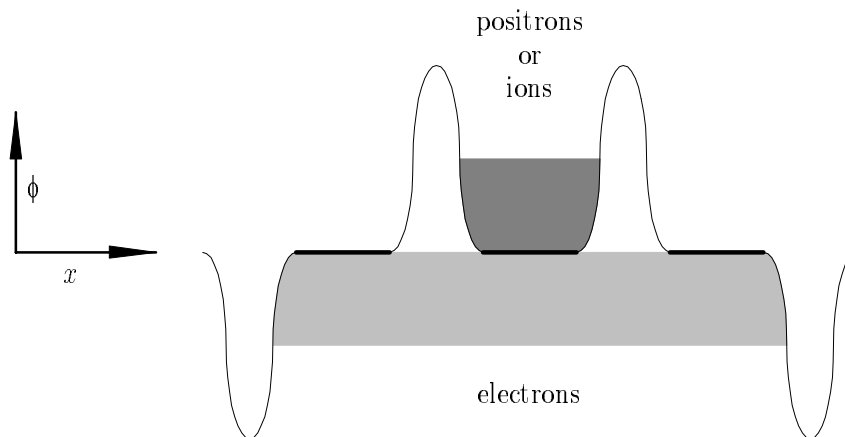


Figure 5.1: The nested well scheme.

This might best be done by using a parabolic or harmonic potential well. In such a well, the bounce motion of all the trapped particles will have the same frequency. An oscillating axial electric field at this frequency would resonantly couple energy into the bounce motion of the trapped particles, driving them out of the well. Any particle which became trapped by collisions or instabilities would be driven out, and the anti-shielding would be maintained.

Much of the recent theoretical work on plasma shielding was done in the context of space physics and satellite based probe design [6, 7, 12, 14]. The results presented in this thesis apply to this field as well. This is due to the fact that much of the near earth plasma is effectively collisionless, thus the fields near a satellite probe will be given by collisionless shielding theory.

## 5.2 Future Research Directions

These experiments were performed only on (effectively) one dimensional non-neutral plasmas. This system is ideal for demonstrating the important features of the theory, but it has several limitations. Understanding these limitations and how they can be alleviated suggests several promising avenues for further research. Some of these are already being pursued. In our lab at present, experiments are being done to test the theory of instantaneous trapping (see Appendix A). Others require different experimental approaches than the ones described here.

Two limitations to our experiment are that it can only trap a plasma of a single

charge species, and that the plasma trapped must be strongly magnetized ( $\omega_c \gg \omega_p$ ). To fully test the theory therefore, the experiments must be extended to the realm of higher dimensional and multi-species plasmas. In particular, it should be possible to test the theory in two and three dimensions by using electrostatic probes of various geometries in discharge type plasmas which are both collisionless and have well characterized velocity distribution functions. Since these are multi species plasmas, the theory will need to be extended as well. The theory of shielding in multi-species plasmas will necessarily be somewhat more complicated than the theory of shielding in a single species plasma. One complicating factor is the fact that the time scales relating to the motion of the different species might differ significantly. Thus a perturbation in a multi-species plasma might be adiabatic to the electrons yet instantaneous to the ions. Both responses will then contribute to the self consistent solution.

This thesis has developed and tested a new theory of plasma shielding. Previous theories of shielding were valid only under limited circumstances. In particular, previous theories of shielding were not valid for collisionless plasmas undergoing adiabatic perturbations. This thesis discusses adiabatic perturbations in detail and describes experiments done to verify the theory of dynamic shielding in single species plasmas. The theory has also been extended to several cases which we could not test experimentally. This work is presented in the hope that it will stimulate future interest in the field of collisionless plasma shielding.

## Appendix A

# Ongoing Modifications

Several modifications to the apparatus described in Chapter 3 are now in progress. These modifications are being made to expand the number of accessible experiments.<sup>1</sup>

### A.1 Fast Perturbations

In Chapter 2 we described a theory of “instantaneous shielding” – a regime of interest where the perturbation is applied on time scales much faster than those relevant to the particle motion. In our case, testing this theory would require pulses with rise times of order 10 ns. As we discussed in Chapter 3 the limit of pulse speed is set by the transmission line which carries the signal into the vacuum chamber and the manner in which it is terminated inside the vacuum chamber. Since the apparatus was not originally designed for high speed signals, these concerns did not play a major role in its original construction. Some of the difficulties are illustrated in Figure A.1.

To improve the high speed characteristics of the experiment, we will modify it in accordance with the following three rules:

1. All transmission lines must have uniform impedance to prevent reflections.
2. All unshielded leads and connections in the signal path have a finite inductance which must be taken into account.
3. There must be a well defined ground to which all electrodes can be referenced.

---

<sup>1</sup>Anita Reimann has provided considerable assistance with these modifications.

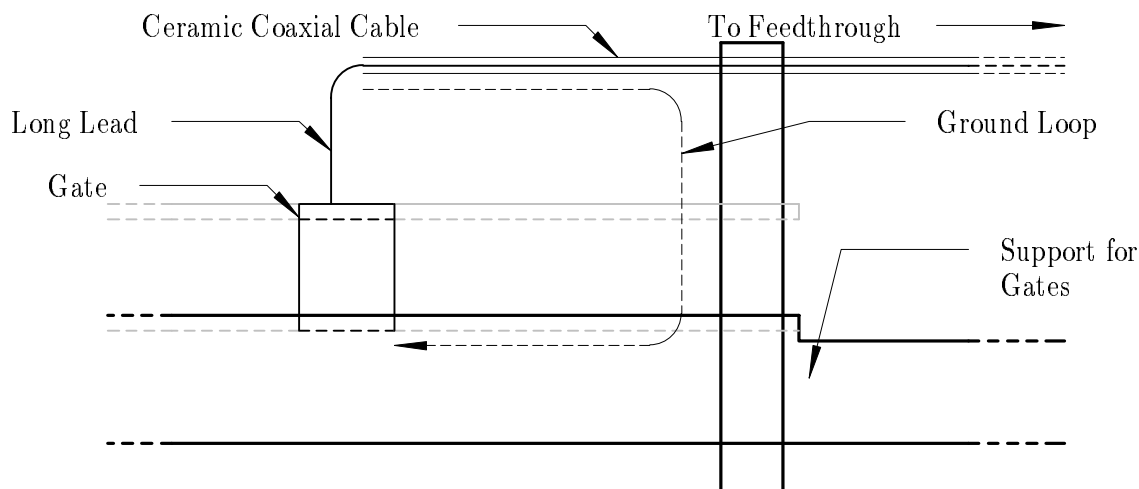


Figure A.1: A diagram of the original construction of the experiment showing some of the difficulties with high speed signals.

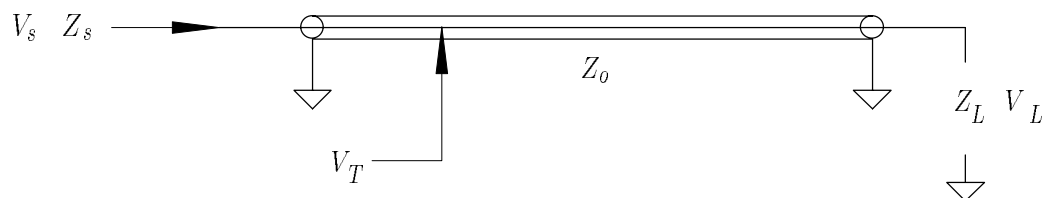


Figure A.2: A schematic of the transmission line and gate

We will therefore make the following modifications:

1. 50 $\Omega$  coaxial cable will be used from the signal source (which will have a 50 $\Omega$  output impedance) to the gate electrode. This was not done originally because the materials out of which 50 $\Omega$  cables are made degrade the vacuum.
2. The support channel for the gates will be used as ground.
3. All cables will terminate with their outer conductor in contact with ground, in this case the support channel, and the shortest possible lead will connect the center conductor to the gate.

The system can now be approximated by the circuit shown in figure A.2.

When the system is assembled it will be impossible to measure the voltage on the gate directly. Even if this were possible, doing so would considerably degrade the response by adding an additional load, making any such measurement useless. To devise a scheme

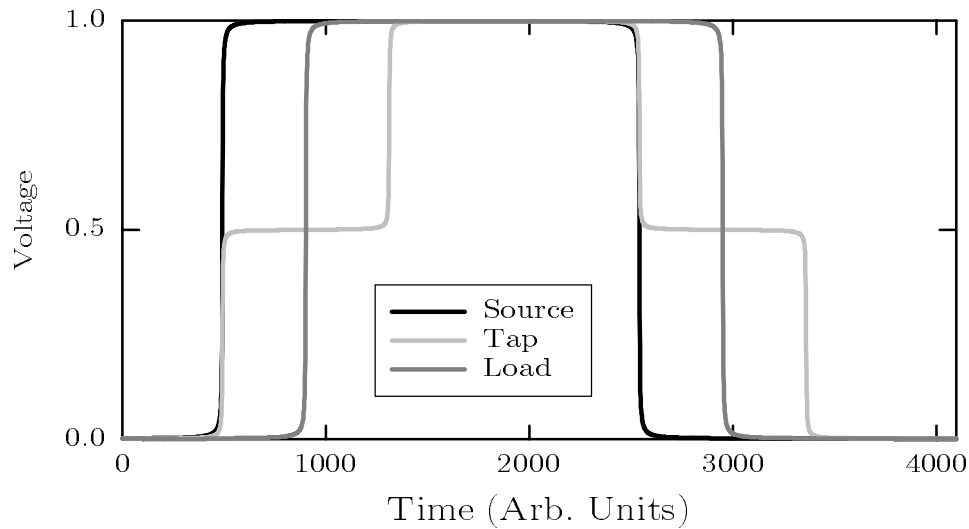


Figure A.3: The response of an open terminated transmission line

by which this can be tested it will be useful to determine in detail how the transmission line will respond to a pulse.

Imagine a pulser with output impedance  $50\Omega$  attached to a  $50\Omega$  impedance cable which is open terminated. At a point along the cable, the voltage as a function of time will consist of a forward and reflected pulse. (See figure A.3) Since the cable is terminated with an impedance  $Z = \infty$  the boundary conditions imply that the forward and reflected voltage pulses will be identical. Note also that the voltage at the end of the cable will simply be a single pulse. If the cable is instead terminated with an arbitrary impedance the response will be modified. It is possible to quantitatively describe the response of such a system. Our goal will be to determine the characteristics of the termination of a transmission line by examining the reflected pulse.

We will suppose that the pulser outputs a voltage  $V_p(t)$  as a function of time and calculate the voltages  $V_L(t)$  at the load and  $V_T(t)$  at a point part way along the cable, which we will refer to as the “tap” voltage. Figure A.2 illustrates the problem. It will be more convenient to work with the Fourier transform of these quantities. Since the system

is linear, we can solve for its behavior at a general frequency  $\omega$ , and then find its response to a general pulse by breaking the pulse down into Fourier components. In this case the voltage and current in a transmission line are related by

$$\begin{aligned} V(\omega, x) &= Z_o [I_i(\omega, x) + I_r(\omega, x)], \\ I(\omega, x) &= I_i(\omega, x) - I_r(\omega, x), \\ I_i(\omega, x) &= I_{oi}(\omega) e^{-j\frac{\omega}{v}x}, \\ I_r(\omega, x) &= I_{or}(\omega) e^{j\frac{\omega}{v}x}, \end{aligned} \tag{A.1}$$

where  $Z_o$  is the transmission line impedance, and  $v$  is the wave velocity of the line. The boundary condition at the load end gives

$$I(\omega, x)Z_L = Z_o [I_i(\omega, x) + I_r(\omega, x)] \tag{A.2}$$

where  $Z_L$  is the load impedance. After some algebra, we find,

$$\frac{I_{or}(\omega)}{I_{oi}(\omega)} = e^{-2i\frac{\omega}{v}x} \left[ \frac{Z_L - Z_o}{Z_L + Z_o} \right]. \tag{A.3}$$

The boundary condition at the source end is

$$V_s(\omega) - [I_{oi}(\omega) - I_{or}(\omega)] Z_s = Z_o [I_{oi}(\omega) + I_{or}(\omega)]. \tag{A.4}$$

We can now use these boundary conditions to solve for  $I_{oi}$  and  $I_{or}$ :

$$\begin{aligned} I_{io}(\omega) &= V_s(\omega) \left[ (Z_o + Z_s) + \frac{(Z_o - Z_s)(Z_L - Z_o)}{(Z_L + Z_o)} e^{-2i\frac{\omega}{v}x} \right], \\ I_{ro}(\omega) &= V_s(\omega) \left[ (Z_o - Z_s) + \frac{(Z_o + Z_s)(Z_L + Z_o)}{(Z_L - Z_o)} e^{2i\frac{\omega}{v}x} \right]. \end{aligned} \tag{A.5}$$

These equations allow us to construct a function relating the source voltage to the voltage anywhere along the transmission line. For example, the response of a transmission line terminated in a capacitor is shown in Figure A.4. We find that the pulse will no longer be a sharp pulse but will instead have an exponential falloff with time constant  $\tau = Z_c C$  where  $Z_c$  is the impedance of the cable and  $C$  is the capacitance of the capacitor at the terminus. It is important to note however, that even in this case, the voltage on the capacitor will consist of a single pulse.

We will now use this model to obtain the electrical characteristics of the gate by finding the best fit to the response of the system to a real pulse. The actual response of the system is shown in Figure A.5, and this response is compared to a best fit model based on propagating the measured output of the pulser through the transmission line equations. Note that the measured pulse is not square, so much of the structure in Figure A.5 is due to the complicated structure of the initial pulse. The best fit parameters are:

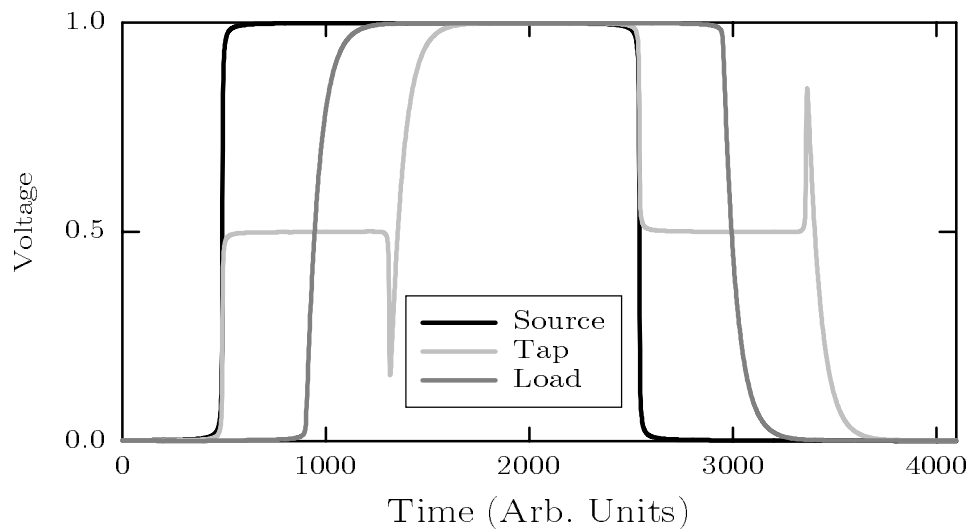


Figure A.4: The response of a transmission line which is terminated with a pure capacitance.

1. Source series inductance:  $3.5 \times 10^{-7}$  H
2. Parasitic source capacitance:  $50 \times 10^{-12}$  F
3. Parasitic source series resistance:  $10\Omega$
4. Load series resistance:  $10\Omega$
5. Load series inductance:  $0.7 \times 10^{-7}$  H
6. Load capacitance:  $120 \times 10^{-12}$  F

The fit to the measured response is good enough to give us confidence that the model parameters accurately describe the electrical characteristics of the gate.

## A.2 Segmented Filament

In Section 3.2 we discussed the fact that the initial density profile of the plasma is determined by the filament voltage distribution, and that at present, only one parameter,

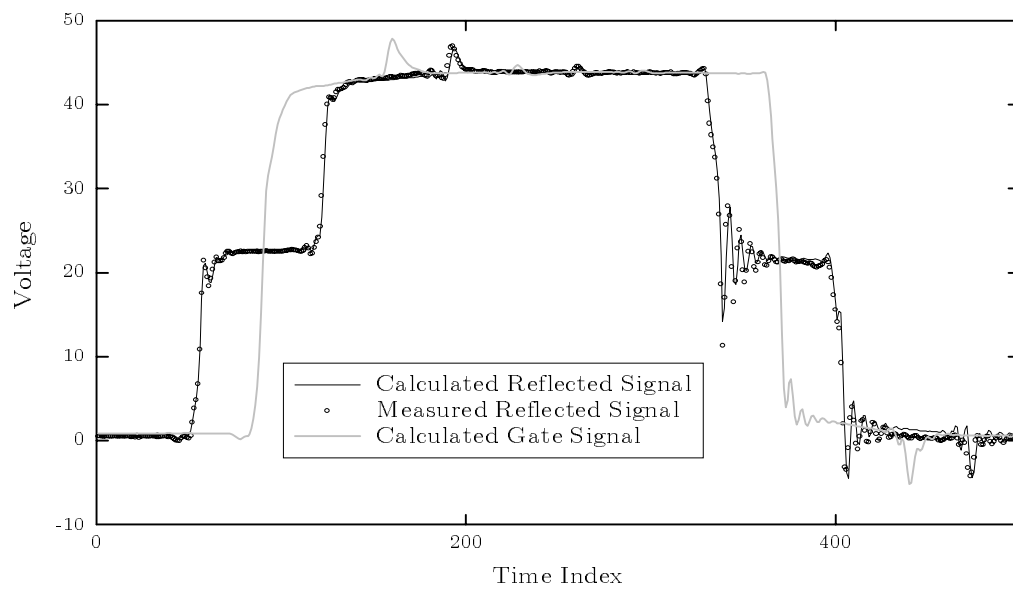


Figure A.5: Comparison between measured and predicted waveforms. The calculated response is based on propagating the measured output of the pulser through the transmission line equations with the parameters listed in the text. The response at the tap and at the gate is calculated. Since the calculated response at the tap can be compared with a measurement, and since this measurement agrees with the calculation, the voltage on the gate must be given by the gray line above. The sampling rate for the traces shown is 500 Ms/s.

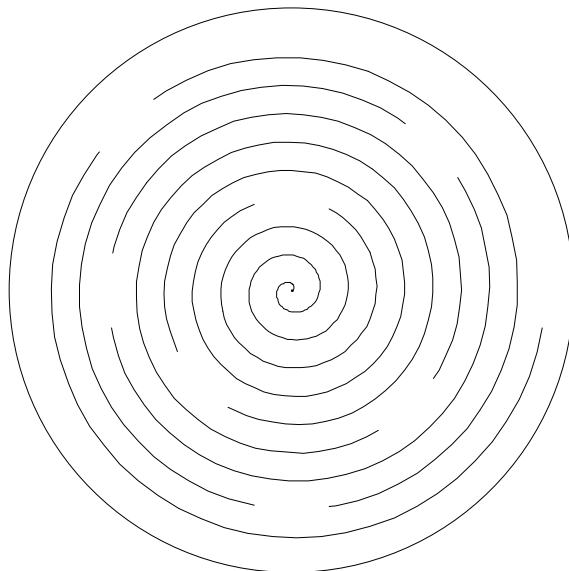


Figure A.6: The layout of the segmented filament

namely the bias potential, can be altered experimentally. To provide a larger variety of initial conditions, and therefore greater experimental flexibility, we will replace the existing filament with a filament consisting of eight segments. Since this filament is broken down into eight segments, we will now have eight parameters with which to affect the radial distribution. We will essentially be able to tailor the radial profile of the plasma by altering the initial boundary conditions. A diagram of this new filament is shown in Figure A.6. The eight segments vary in length from 1.62 in. to 2.41 in. Each is made from Tungsten wire of thickness 0.020 inches. They are wound in sections of a spiral with pitch 0.075 inches per turn.

The installation of this new filament will require several additional modifications. These are necessitated by the greater structural and electrical complexity of the new filament as well as its larger power consumption and hence cooling requirements. The elements supporting the filament are shown in Figure A.7

### A.3 Vision System

The final upgrade to the experiment which is now being undertaken constitutes a major change to the diagnostics available. At present, the radial distribution of plasma is

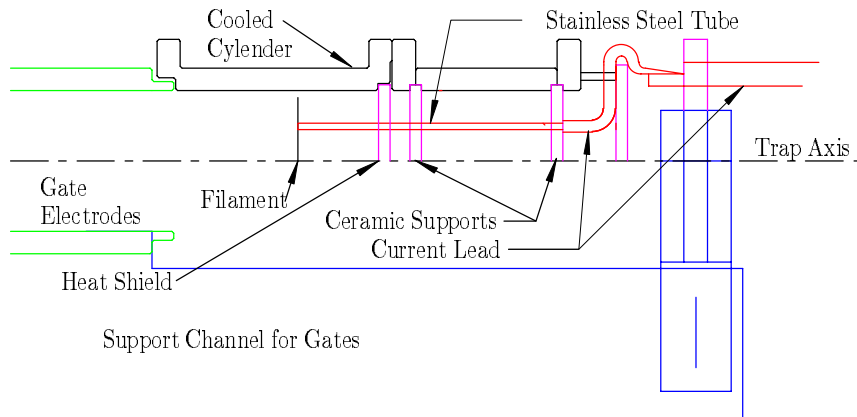


Figure A.7: Drawing showing the installation of the segmented filament

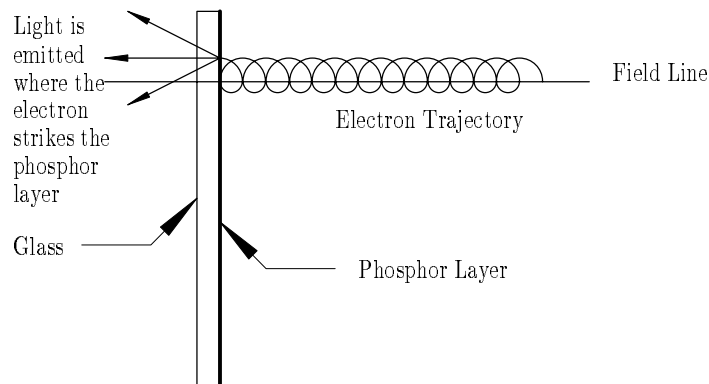


Figure A.8: A diagram of the phosphor screen diagnostic

determined using the movable pinhole diagnostic. This will be replaced with a phosphor screen and camera. The advantage of a phosphor screen is that it will allow the entire radial distribution of charge to be measured with a single shot. This imaging system replaces one originally designed by Tony Peurrung [33, 34]

Like the movable pinhole diagnostic, the phosphor screen diagnostic is destructive. It works by allowing the plasma electrons to strike an electroluminescent phosphor after they are released from the confinement region. The phosphor screen gives off an amount of light which is proportional to the number of electrons which hit it. Since the electrons stream along magnetic field lines, the amount of light released is proportional to the electron density inside the trap. This light can then be imaged with a CCD camera. This process is shown in figure A.8.

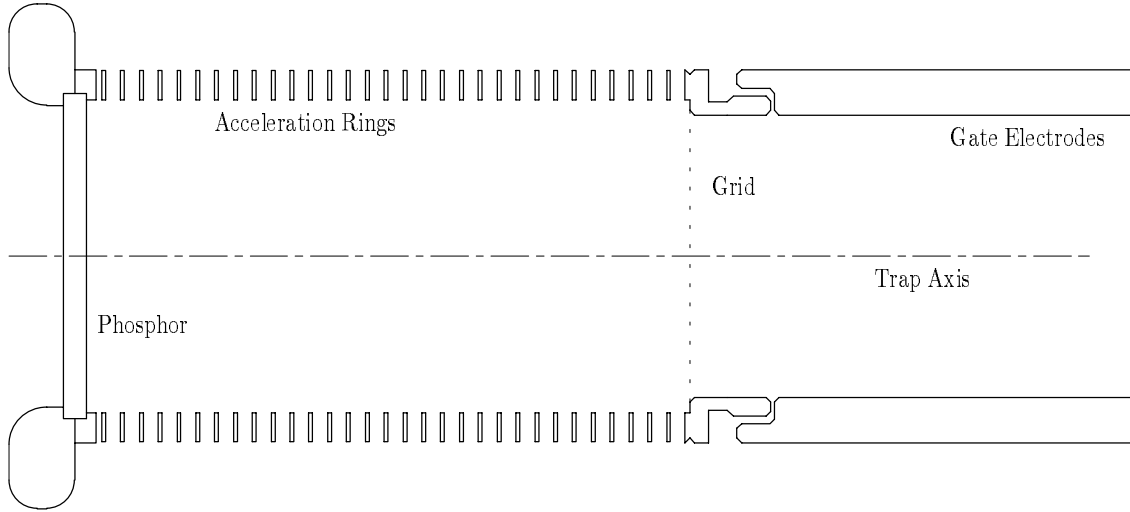


Figure A.9: The electrode configuration used for electron acceleration

In order for the electrons to generate sufficient light to be easily detectable with the CCD camera, they must be accelerated to greater than 5 or 10 keV, possibly as high as 30 keV. To accomplish this, we will bias the phosphor to a very large positive value. Since any electric field which is perpendicular to the magnetic field will cause an  $\mathbf{E} \times \mathbf{B}$  drift we want to ensure that the electric field is entirely parallel to the magnetic field. This is accomplished by using the electrode configuration shown in figure A.9. The phosphor and the grid form planar equipotentials. The side rings are biased in such a way as to keep the field as uniform as possible. Since the grid will be held near ground, the fields will not penetrate into the plasma confinement region. Though the scheme does prevent large scale non-uniformities in the electric field, it does so by introducing small scale non-uniformities. This will be especially true in the region very near the grid and in the region at the edge near the rings. We must calculate how large these electric fields will be and their consequences on an electron to insure that the trajectories of the electrons and thus the image of the plasma will not be adversely affected. We will first estimate the effect of the fields due to the grid on a drifting electron.

Imagine an electron tied to a magnetic field line, moving with uniform velocity  $v_{\parallel}$  approaching a single wire with charge per unit length  $\lambda$  which lies perpendicular to the magnetic field. This electron will see an electric field due to the line charge on the wires. The component of this field perpendicular to  $\mathbf{B}$  will cause an  $\mathbf{E} \times \mathbf{B}$  drift. The total distance

this electron will drift will be

$$\Delta x = \int_{-\infty}^{\infty} \frac{\lambda}{2\pi\epsilon_o B v_{\parallel}} \frac{b}{b^2 + y^2} \frac{1}{y} dy. \quad (\text{A.6})$$

Where  $b$  is the distance of closest approach. In general,  $v_{\parallel}$  depends strongly on the potentials on the grid. To make an order of magnitude estimate of the drift, however, we can estimate  $v_{\parallel}$  with

$$\frac{1}{2} m_e v_{\parallel}^2 \sim \frac{e\lambda}{2\pi\epsilon_o} \ln\left(\frac{a}{b}\right). \quad (\text{A.7})$$

where  $a$  is the spacing between the wires. If the phosphor potential is  $\phi_a$  and the length of the region is  $\ell$ , this wire is part of a grid with electric field

$$E_a = \frac{\phi_a}{\ell} \quad (\text{A.8})$$

on one side and no field on the other side,  $\lambda$  is given simply by

$$\lambda = a \frac{\phi_a}{\ell} \epsilon_o. \quad (\text{A.9})$$

Therefore,

$$\Delta x \sim \frac{\phi_a a}{B v_{\parallel} \ell}, \quad (\text{A.10})$$

and

$$v_{\parallel} \sim \frac{1}{m_e} \sqrt{\frac{ea\phi_a}{2\pi\ell} \ln(a/b)}. \quad (\text{A.11})$$

Substituting,

$$\Delta x \sim \frac{1}{B} \sqrt{\frac{2\pi a\phi_a}{e\ell \ln(a/b)}} \quad (\text{A.12})$$

To minimize  $\Delta x$  therefore, we want to minimize the ratio  $a/\ell$ . There is one other important condition. We want to ensure that the electric field near the surface of the wires is not so large that the electrons are pulled off of field lines:

$$E_{max} = \frac{\phi_a a}{2\pi r_w \ell} \ll cB, \quad (\text{A.13})$$

where  $r_w$  is the radius of the wire. This relation puts an upper limit on the ratio  $a/r_w \ell$ .

Therefore, given an acceptable  $\Delta x$ , we obtain the approximate relations,

$$\frac{a}{\ell} \sim \frac{B^2 (\Delta x)^2 e}{m_e \phi_a} \quad (\text{A.14})$$

and

$$\frac{r_w \ell}{a} \gg \frac{\phi_a}{2\pi cB} \quad (\text{A.15})$$

For  $B = 0.2T$ ,  $\phi_a = 10kV$  and  $\Delta x = 2 \times 10^{-4}m$ , we find that  $a/\ell = 0.028$ , and  $r_w\ell/a \gg 2.6 \times 10^{-5}m$ . The design we plan to adopt will have  $a/\ell = 0.016$  and  $r_w\ell/a = 1.6 \times 10^{-3}m$ .

The rings bounding the sides of the acceleration region will also have an effect. The magnitude of this effect can be estimated as follows. In the interior of the acceleration region we must have

$$\nabla^2\phi = 0. \quad (\text{A.16})$$

In the region at the edge of the acceleration region, very close to the rings, there is approximately rectangular symmetry. We will therefore assume rectangular symmetry to simplify the calculation. We will assume that the nonuniformities are periodic in  $x$ , i. e.

$$\phi(x, y) = E_a x + \sum_j \left[ A_j(y) \cos\left(\frac{2\pi j x}{\delta}\right) + B_j(y) \sin\left(\frac{2\pi j x}{\delta}\right) \right]. \quad (\text{A.17})$$

We must therefore have

$$\frac{A_j''(y)}{A_j(y)} = \left(\frac{2\pi j}{\delta}\right)^2. \quad (\text{A.18})$$

Therefore,

$$A_j(y) = A_{oj} \exp\left(\frac{-2\pi j y}{\delta}\right), \quad (\text{A.19})$$

where the exponentially growing solution has been discarded as unphysical (it can not match the boundary condition at the center of the trap because its derivative will not be continuous there). The solution for  $B_j(y)$  is similar.

We see immediately that the spacing between the rings sets the scale for the nonuniformities they cause. It is therefore advantageous to have the rings spaced as close together as possible. We will now try to approximate the size of the various Fourier coefficients. We will begin by making a simple approximation, namely that for rings of thickness  $t$ , the voltage perturbation can be written

$$\begin{aligned} \phi_p(x) &= \frac{E_a t}{2} \frac{x}{\delta/2 - t/2} & \text{for } |x| \leq \delta/2 - t/2 \\ \phi_p(x) &= \frac{E_a t}{2} \left( 1 - \frac{2|x - (\delta/2 - t/2)|}{t} \right) & \text{for } \delta/2 - t/2 < |x| \leq \delta \end{aligned} \quad (\text{A.20})$$

The Fourier coefficients are therefore

$$\begin{aligned} A_{oj} &= 0 \\ B_{oj} &= \frac{2}{\delta} \int_0^\delta \phi_p(x) \sin\left(\frac{2\pi j x}{\delta}\right) dx. \end{aligned} \quad (\text{A.21})$$

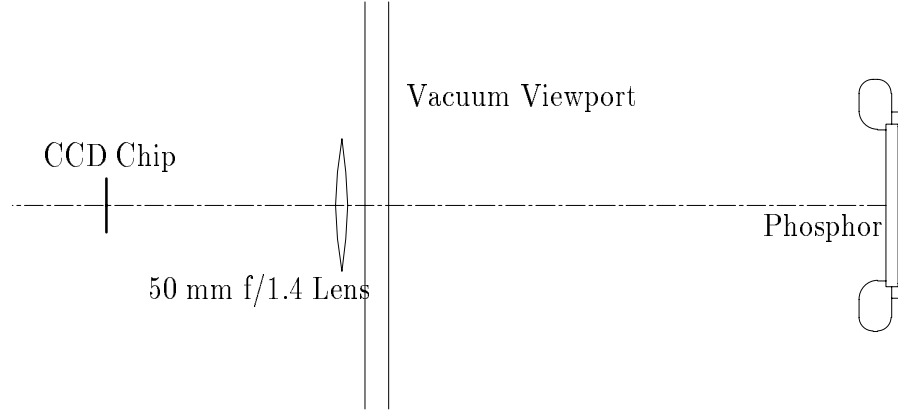


Figure A.10: The phosphor optics

Note that  $A_{oj}$  vanishes due to the fact that we have picked the zero of  $x$  such that  $\phi_p(x)$  is odd. Evaluating the above, we find that

$$B_{oj} = \frac{E_a t}{\pi j} \quad (\text{A.22})$$

for  $t/d \ll 1$  and  $j \ll \delta/t$ . To lowest order, therefore, the radial electric field is

$$E_r = \frac{2E_a t}{\delta} \sin\left(\frac{2\pi j x}{\delta}\right) \exp\left(\frac{-2\pi j y}{\delta}\right). \quad (\text{A.23})$$

We will therefore have a large number of closely spaced thin rings to establish the boundary condition. We will also ensure that the streaming plasma does not approach the walls of the acceleration region too closely. The present design calls for  $\delta/t \simeq 5$  and the closest distance the plasma will approach the walls will be  $\simeq 0.82\delta$ . Therefore the maximum nonuniformity in the electric field due to the rings will be approximately 0.2 %.

The phosphorescent material itself forms a thin layer which is bonded to a piece of glass. The light from the phosphor can therefore propagate through the glass, through a transparent window in the vacuum chamber, to be imaged by the CCD camera. The optical path is shown in figure A.10. The CCD camera digitizes the picture so that it can be analyzed.

## A.4 Current Progress

At the time of this writing, the fast perturbation scheme has proven successful [19]. We are now in the process of removing it so that the segmented filament and the

vision system can be installed. The design of both of these systems is complete and all of the requisite components have been obtained. The installation should be complete by December 1996.

## Appendix B

# Glossary

**adiabatic** A perturbation is adiabatic if it occurs slowly compared to the orbital motion of the plasma particles.

**adiabatic invariant** Any quantity which remains constant during an adiabatic perturbation.

**Adiabatically Created Test Well (ACTW)** A well which is created adiabatically. Also referred to as an **elevator scheme**. This is generally contrasted with a **non-Adiabatically Created Test Well (non-ACTW)** which is also known as a **flood scheme**.

**bounce action** or **bounce invariant**. The adiabatic invariant associated with the action variable of the axial (or “bounce”) motion of the electrons.

**collimated** Collimated cylinders are cylinders with identical radii lying adjacent to one another which are axially aligned.

**dimension of a perturbation** The number spatial coordinates necessary to specify the relation of a plasma particle to a perturbation. For example, a one dimensional perturbation can be either any perturbation in a plasma where the particles are restricted to move only along lines, or it could be a plane charge perturbation in a three dimensional plasma where two of the spatial coordinated can be ignored. Likewise a two dimensional perturbation could be a point perturbation in a plasma where the particles are restricted to motion in a plane, or a line charge perturbation in a three dimensional plasma.

**diocotron mode** The first order azimuthal mode ( $\ell = 1$ ) of a non-neutral plasma in a Penning-Malmberg trap, consisting of a displacement of the plasma off of the axis of the trap. The charge centroid of the plasma then rotates about the axis of the trap with a characteristic **diocotron frequency** which depends on the geometry of the trap, the magnetic field and the density of the plasma. (See ref [28] for details.)

**dynamic shielding** The theory which describes how a plasma shields an **adiabatic** perturbation.

**elevator scheme** A perturbation scheme using an **adiabatically created test well**

**flood scheme** A perturbation scheme using a **non-adiabatically created test well**

**free charge** Particles which lie on unbounded orbits.

**instantaneous shielding** The theory which describes how a plasma shields a perturbation which is created rapidly compared to the orbital time scale. This type of perturbation differs from a **non-adiabatically created test well** in that plasma is present when the perturbation is created.

**non-Adiabatically Created Test Well (non-ACTW)** A test well created in a region with no plasma present into which plasma is allowed to flow. This is also referred to as a **flood scheme**. See **Adiabatically Created Test Well**

**non-neutral plasma** A plasma consisting of either positively or negatively charged particles but not both, generally (though not necessarily) a single species.

**passing charge** Particles whose orbits allow them to leave the perturbation. Particles which lie on **passing orbits**.

**passing orbits** Orbits which do not close inside a perturbation region. These orbits may be bounded if the plasma is confined.

**Penning-Malmberg trap** One of many types of non-neutral plasma traps. See Section 3.1 for more details.

**potential hill** A perturbation in a plasma that creates a region of positive potential energy, such as a negative voltage perturbation in an electron plasma. A potential hill has the opposite sign as a **potential well**.

**potential well** A perturbation in a plasma that creates a region of negative potential energy, such as a positive voltage perturbation in an electron plasma. A potential well has the opposite sign as a **potential hill**.

**shielding efficacy** A quantification of the degree of shielding of a perturbation, defined as  $1 - \Phi/\Phi_w$  where  $\Phi_w$  is the applied potential and  $\Phi$  is the net potential (applied plus space charge.) A shielding efficacy of one corresponds to perfect shielding, while a shielding efficacy of zero corresponds to no shielding. Negative shielding efficacies correspond to anti-shielding.

**trapped charge** Particles whose orbits do not allow them to leave a perturbation region. Particles which lie on **trapped orbits**.

**trapped orbits** Orbits which close inside a perturbation region. In an infinite plasma with a single perturbation, all bounded orbits are trapped orbits.

# Bibliography

- [1] Francis F. Chen. *Plasma Physics and Controlled Fusion*. Plenum Press, New York, 1984.
- [2] D. R. Nicholson. *Introduction to Plasma Theory*. John Wiley and Sons, New York, 1983.
- [3] E. W. Laing, A. Lamont, and P. J. Fielding. Interaction of test particles with a plasma. *J. Plasma Phys.*, 5:441, 1971.
- [4] D. Montgomery and F. Tappert. Conductivity of a two-dimensional guiding center plasma. *Phys. Fluids*, 15:683, 1972.
- [5] E. W. Laing and A. L. Gibson. Interaction of a test particle with a magnetized plasma. *J. Plasma Phys.*, 14:433, 1975.
- [6] P. Chenevier, J. M. Doloique, and H. Peres. Potential created by a test particle in one-, two-, and three-dimensions in a flowing ion-electron plasma. *J. Plasma Phys.*, 10:185, 1973.
- [7] A. V. Gurevich. Distribution of captured particles in a potential well in the absence of collisions. *Sov. Phys. JETP*, 26:575, 1968.
- [8] M. Psimopoulos and D. Lee. Cross field thermal transport in highly magnetized plasmas. *Proc. Royal Soc. Lond.*, 437:55, 1992.
- [9] M. Psimopoulos and A. Rogister. Density of untrapped electrons near a particle of a plasma. *Phys. Lett. A*, 149:265, 1990.
- [10] M. Psimopoulos. The velocity distribution and the density near a particle of an equilibrium one component plasma. *Phys. Lett. A*, 88:172, 1982.

- [11] M. Psimopoulos. The velocity distribution and the density near a particle of an equilibrium two component plasma. *Phys. Lett. A*, 88:176, 1982.
- [12] N. M. Meyer-Vermet. Aspects of Debye shielding. *Am. J. Phys.*, 61:249, 1993.
- [13] E. Lifshitz and L. Pitaevskii. *Physical Kinetics*. Pergamon, New York, 1981.
- [14] J. G. Laframboise and L. W. Parker. Probe design for orbit-limited current collection. *Phys. Fluids*, 16:629, 1973.
- [15] B. Abraham-Shrauner. Test particle in a two-dimensional plasma. *Physica*, 43:95, 1969.
- [16] C. Hansen and J. Fajans. Dynamic and Debye shielding and antishielding in magnetized, collisionless plasmas. *Phys. Rev. Lett.*, 74:4209, 1995.
- [17] J. D. Moody and C. F. Driscoll. Rarefaction waves, solitons, and holes in a pure electron plasma. *Phys. Plasmas*, 2:4482, 1995.
- [18] S.C. Neu and G.J. Morales. Propagation of nonlinear pulses in a non-neutral plasma. *Phys. Plasmas*, 2:3033, 1995.
- [19] A. Reimann, C. Hansen, and J. Fajans. *Bull. Am. Phys. Soc.*, To be published.
- [20] J. H. Malmberg, C. F. Driscoll, B. Beck, D. L. Eggleston, J. Fajans, K. Fine, X. P. Huang, and A. W. Hyatt. Experiments with pure electron plasmas. In C.W. Roberson and C.F. Driscoll, editors, *Nonneutral Plasma Physics*, volume AIP 175, page 28, New York, 1988. American Institute of Physics.
- [21] J. Fajans and D. H. E. Dubin, editors. *Non-Neutral Plasma Physics II*, volume AIP 331. American Institute of Physics, New York, 1995.
- [22] T. M. O'Neil. A confinement theorem for nonneutral plasmas. *Phys. Fluids*, 23:2216, 1980.
- [23] J. H. Malmberg and J. S. deGrassie. Properties of a nonneutral plasma. *Phys. Rev. Lett.*, 35:577, 1975.
- [24] C. F. Driscoll and J. H. Malmberg. Hollow electron column from an equipotential cathode. *Phys. Fluids*, 19:760, 1976.

- [25] J. S. DeGrassie and J. H. Malmberg. Waves and transport in the pure electron plasma. *Phys. Fluids*, 23:63, 1980.
- [26] A. J. Peurrung and J. Fajans. Non-neutral plasma shapes and edge profiles. *Phys. Fluids B*, 2:693, 1990.
- [27] K. S. Fine. *Experiments with the  $l=1$  Diocotron Mode*. PhD thesis, University of California, San Diego, 1988.
- [28] K. S. Fine, C. F. Driscoll, and J. H. Malmberg. Measurements of a nonlinear diocotron mode in pure electron plasmas. *Phys. Rev. Lett.*, 63:2232, 1989.
- [29] K. S. Fine. Simple theory of a nonlinear diocotron mode. *Phys. Fluids B*, 4:3981, 1992.
- [30] D. L. Eggleston, C. F. Driscoll, B. R. Beck, A. W. Hyatt, and T. H. Malmberg. Parallel energy analyzer for pure electron plasma devices. *Phys. Fluids B*, 4:3432, 1992.
- [31] J. P. Verboncoeur, A. B. Langdon, and N. T. Gladd. An object-oriented electromagnetic pic code. *Comp. Phys. Comm.*, 87:199, 1995.
- [32] I. B. Bernstein, J. M. Greene, and M. D. Kruskal. *Phys. Review*, 108:546, 1969.
- [33] A. J. Peurrung, J. Notte, and J. Fajans. Imaging of a nonneutral plasma. *Bull. Am. Phys. Soc.*, 36:2332, 1991.
- [34] A. J. Peurrung. *Imaging of Instabilities in a Pure Electron Plasma*. PhD thesis, University of California, Berkeley, 1992.